



1 Product Ion Distributions using H_3O^+ PTR-ToF-MS: Mechanisms, 2 Transmission Effects, and Instrument-to-Instrument Variability

3 Michael F. Link¹, Megan S. Claflin², Christina E. Cecelski¹, Ayomide A. Akande³, Delaney Kilgour⁴,
4 Paul A. Heine³, Matthew Coggon⁵, Chelsea E. Stockwell⁵, Andrew Jensen^{6,a}, Jie Yu⁷, Han Huynh^{7,b},
5 Jenna C. Ditto^{7,c}, Carsten Warneke⁵, William Dresser⁶, Keighan Gemmell³, Spiro Jorga^{7,d}, Raleigh L.
6 Robertson^{1,e}, Joost de Gouw⁶, Timothy Bertram⁴, Jonathan P.D. Abbatt⁷, Nadine Borduas-Dedekind³,
7 Dustin Poppendieck¹

8 ¹National Institute of Standards and Technology, Gaithersburg, 20899, USA

9 ²Aerodyne Inc., Billerica, 01821, USA

10 ³Department of Chemistry, University of British Columbia, Vancouver, V6T 1Z1, Canada

11 ⁴University of Wisconsin-Madison, Madison, 53706, USA

12 ⁵National Oceanic and Atmospheric Administration, Boulder, 80305, USA

13 ⁶University of Colorado, Boulder, 80309, USA

14 ⁷University of Toronto, Toronto, M5S 3H6, Canada

15 ^aNow at University of Michigan, Ann Arbor, 48109, USA

16 ^bNow at National Oceanic and Atmospheric Administration, Boulder, 80305, USA

17 ^cNow at Washington University in St. Louis, 63130, USA

18 ^dNow at Tofwerk, Thun, 3645, Switzerland

19 ^eNow at University of Colorado, Boulder, 80309, USA

20
21 *Correspondence to:* Michael F. Link (michael.f.link@nist.gov)

22 **Abstract.** Proton-transfer-reaction mass spectrometry (PTR-MS) using hydronium ion (H_3O^+) ionization is widely used for
23 the measurement of volatile organic compounds (VOCs) both indoors and outdoors. Unlike more energetic ionization methods
24 (e.g., electron impact), H_3O^+ ionization can leave a target VOC molecule mostly intact and thus a VOC in a PTR-MS mass
25 spectrum can be identified by its mass-to-charge ratio corresponding to the proton-transfer product (MH^+). However, H_3O^+
26 ionization, and associated chemistry in the ion molecule reactor, is known to generate other product ions besides the proton-
27 transfer product. The product ion distributions (PIDs) created during ionization include ions resulting from charge transfer
28 reactions, water clustering, and fragmentation, all of which can create ambiguity when interpreting PTR-MS mass spectra. A
29 standardized method of evaluating and quantifying the possible influence of PIDs on PTR-MS mass spectra is limited in part
30 due to an incomplete understanding of the formation mechanisms and effects of instrument settings on measured PIDs, as well
31 as the reasons for instrument-to-instrument variability.

32
33 We present a method, using gas-chromatography pre-separation, for quantifying PIDs from PTR-MS measurements of
34 nearly 100 VOCs of different functional types including alcohols, ketones, aldehydes, acids, aromatics, halogens, and



35 alkenes. Using this method we highlight major contributions of water cluster and fragment product ions to the PIDs of
36 oxygenated VOCs. We characterize the influence of ion-molecule reactor conditions, ion transmission effects from
37 quadrupole and ion optic tuning, and inlet capillary configuration on measured PIDs. We find that reactor conditions have
38 the strongest impact on measured PIDs, but ion optic voltage differences and inlet capillary configuration can also affect
39 PIDs.

40
41 Through an interlaboratory comparison of PIDs measured from calibration cylinders we characterize the variability of PID
42 production from the same model of PTR-MS across seven participating laboratories. A subset of VOCs measured by the
43 different laboratories had standard deviations (1σ) associated with product ions that varied no more than 20 % thus
44 providing a constraint for predicting PIDs across instruments operating under different conditions. We highlight the potential
45 for misidentification of VOCs in PTR-MS mass spectra with a case study measurement of restroom air. We propose methods
46 for identifying likely product ions and constraining the influence of PIDs on PTR-MS mass spectra. Finally, we present a
47 library of H_3O^+ PIDs, from measurements acquired as part of this study, to be publicly available and updated periodically
48 with user-provided data for the continued investigation into instrument-to-instrument variability of PIDs.

49 **1 Introduction**

50 Measurements of volatile organic compounds (VOCs) using hydronium ion (H_3O^+) proton-transfer-reaction mass spectrometry
51 (PTR-MS) have become ubiquitous in a variety of applications in the past 25 years (Yuan et al., 2017; Sekimoto and Koss,
52 2021). PTR-MS can measure many VOCs simultaneously with fast (> 1 Hz) time resolution and low detection limits (e.g., $<$
53 1 nmol mol^{-1}), and is selective towards VOCs that have a proton-affinity greater than water (e.g., ketones, aldehydes, nitriles,
54 etc.) (De Gouw et al., 2003). However, in the absence of sample pre-separation, isobaric (i.e., same mass-to-charge ratio, m/Q)
55 interferences are known to pose challenges to VOC identification and quantification (Coggon et al., 2024; Kilgour et al., 2024).
56 Since the early development of PTR-MS, studies have shown that unintended product ions can complicate mass spectra
57 (Warneke et al., 2003; De Gouw and Warneke, 2007), but more recent studies have highlighted ion interferences in
58 measurements of urban air plumes (Coggon et al., 2024) and indoor air (Ernle et al., 2023) where interferences are pronounced
59 because VOC concentrations are high and emission sources are diverse. As PTR-MS technology continues to improve through
60 the development of new sample introduction methods, ionization technologies (Krechmer et al., 2018; Breitenlechner et al.,
61 2017; Reinecke et al., 2023), and enhanced mass resolution through the use of time-of-flight mass analyzers, this method will
62 continue to be utilized in concentrated and chemically diverse sample matrices. The popularity of this measurement technique
63 warrants the creation of standardized methods for measuring and quantifying the effects of unintended, or poorly understood,
64 product ion distributions on PTR-MS mass spectra.

65



66 Unintended product ion generation in PTR-MS has been discussed extensively including studies highlighting the importance
67 of VOC fragmentation from H_3O^+ ionization (e.g., aldehydes (Ernle et al., 2023), peroxides (Li et al., 2022), and monoterpenes
68 (Miształ et al., 2012)) and studies using selected-ion flow tube (SIFT) reaction measurements (summarized in a recent review
69 by Hegen et al. (2023)) to differentiate interferences from O_2^+ and NO^+ reagent ion impurities. Pagonis et al. (2019) presented
70 a library of previously reported product ion distributions (PIDs) compiled from measurements of VOCs. However, water
71 cluster contributions to the PIDs were largely not incorporated in this compilation. The library shows considerable variability
72 in the generation of product ions for a given VOC (e.g., butanal, ethyl acetate, etc.), but from the existing data it is not clear if
73 this variability is explained by instrument operating parameters, features of the specific instrument, or methods of quantifying
74 PIDs.

75

76 In this study we highlight:

- 77 (1) a gas chromatographic method for measuring PIDs from the ionization of VOCs using PTR-MS (Section 2.2),
- 78 (2) how instrument configurations can influence PIDs (Section 3.1),
- 79 (3) instrument-to-instrument variability in measured PIDs determined from an interlaboratory comparison (Section 3.2),
- 80 (4) the propensity of different VOC functional types to form complex PIDs that include water clusters (Section 3.3),
- 81 (5) an example of how PIDs can cause ambiguity when identifying ions using a sample of restroom air as a case study (Section
82 3.4),
- 83 (6) suggestions of how PIDs can be used to aid in identification and quantification of VOCs from PTR-MS mass spectra
84 (Section 3.5),
- 85 (7) and a library of H_3O^+ PIDs available for community use, to be updated with continued collaborative input.

86 **2 Materials and Methods**

87 **2.1 Product Ion Definitions and Formation Mechanisms**

88 We use observations from previous studies (Koss et al., 2016; Xu et al., 2022; Pagonis et al., 2019; Hegen et al., 2023; Coggon
89 et al., 2024; Li et al., 2024) to identify the reactions, and associated product ions, that are likely to be important from H_3O^+
90 ionization of a given VOC. The reaction mechanisms we identify here do not represent an exhaustive accounting of possible
91 product ion formation mechanisms, but instead represent mechanisms most likely to generate the product ions observed from
92 our data. VOCs ($M = \text{VOC}$) with a proton-affinity greater than water (691 kJ mol^{-1}) can undergo a proton-transfer reaction
93 with H_3O^+ to form an H^+ adduct (labelled as MH^+) as described in Reaction 1.





95 Unique from most previous studies, we quantify the contribution of protonated VOC water clusters (labelled as $[MH \cdot (H_2O)_n]^+$
96 where $n = 1$ or 2) to the product ion distribution that potentially form from direct association reactions following Reaction 2
97 (Li et al., 2024) and/or termolecular association reactions of a protonated VOC with water vapor following Reaction 3.



100 The presence of a collisional body, B ($B = N_2$ or O_2), in Reactions 2 and 3 implies a pressure-dependence (McCrumb and
101 Warneck, 1977; Smith et al., 2020). Direct protonation and water cluster formation can also occur from reaction of VOCs with
102 reagent ion water clusters (De Gouw and Warneke, 2007).



105 However, the addition of the RF-only quadrupole around the IMR serves to decrease the influence of higher-order water
106 clusters on ionization chemistry (Krechmer et al., 2018). We note that unlike other PTR-MS instruments, the Vocus PTR-ToF-
107 MS instruments featured in this study have been observed to have ionization chemistry that is not appreciably sensitive to
108 sample water vapor concentrations (Krechmer et al., 2018; Li et al., 2024) potentially implying a more predictable influence
109 of water cluster contributions to PIDs.

110 Fragmentation of a protonated VOC can occur from the loss of neutral constituents (e.g., H_2O , CO , and $C_2H_4O_2$) and/or the
111 dissociation of carbon-carbon bonds (Pagonis et al., 2019). We refer to product ions that result from a fragmentation reaction
112 where water is lost from the protonated VOC, following Reaction 6, as dehydration products (labelled as $[MH-H_2O]^+$).

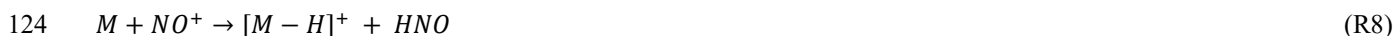


114 We highlight the formation of dehydration products because this fragment ion contributed the most to a PID of an oxygenated
115 VOC. Because other fragmentation product ions could form through a variety of mechanisms, we label other fragmentation
116 product ions as F_n where $n = 1, 2, 3$, etc.

117 We highlight two other reaction mechanisms, charge transfer and hydride transfer, that are responsible for generating product
118 ions that often appear in PTR-MS mass spectra. Charge transfer reactions, between a VOC and impurity reagent ions like O_2^+
119 and NO^+ , can form product ions (labelled as M^+) that appear in the mass spectrum as ionized VOCs with no changes to
120 elemental composition (Reaction 7).



122 Reactions with NO^+ can also ionize VOCs via hydride transfer (labelled as $[M-H]^+$; Reaction 8) (Koss et al., 2016; Španěl and
123 Smith, 1997).



125 We note that Hegen et al. (2023) recently proposed that product ions appearing in mass spectra as hydride transfer products
126 from reactions with O_2^+ may actually be charge transfer products that lose a neutral hydrogen atom. For the purposes of this
127 study we classify any product ion that appears in the mass spectrum with the formula $[M-H]^+$ as a hydride transfer product.
128 NO^+ and O_2^+ ion chemistry can also produce additional product ions through other mechanisms (e.g., hydroxide transfer) not
129 discussed here, but which are summarized in Hegen et al. (2023).

130 We use the above mechanisms for defining the main product ions considered in our analysis and the rules for determining their
131 location in the mass spectrum, relative to the molecular weight (MW) of the VOC, when calculating PIDs (Table 1).

132 **Table 1: Definitions of product ions that occur in PTR-MS mass spectra.**

| Product Ion Identity | Product Ion Label | Mass-to-Charge Ratio (Th) ^a |
|-----------------------|----------------------------------|--|
| H ⁺ adduct | MH ⁺ | MW + 1.007 |
| single water cluster | $[MH \cdot H_2O]^+$ | MW + 19.018 |
| double water cluster | $[MH \cdot (H_2O)_2]^+$ | MW + 37.028 |
| charge transfer | M ⁺ | MW - 0.001 |
| hydride transfer | $[M-H]^+$ | MW - 1.007 |
| dehydration | $[MH-H_2O]^+$ | MW - 18.011 |
| fragment | F _n , n = 1 through 5 | variable |
| other | other | variable |

133 ^aWe express mass-to-charge ratio (m/Q) in units of Thomson (Th) which is equal to $1.0364 \times 10^{-8} \text{ kg C}^{-1}$.

134 For our analyses we limited the total number of fragment ions that contribute to a PID to five. Most VOCs did not generate
135 more than two fragment ions. Some VOCs (e.g., aromatics generating $C_6H_7O^+$) generated product ions that were consistently
136 observed, but we could not easily explain how they formed and so we classify these few ions as “other”.



137 2.2 Method of Quantifying PIDs from GC-PTR-ToF-MS Measurements

138 2.2.1 Measurement of PIDs using Gas Chromatography Proton-Transfer-Reaction Time of Flight Mass Spectrometry 139 (GC-PTR-ToF-MS)

140 We used gas-chromatography (GC) pre-separation as a technique for isolating VOCs from multi-component standards before
141 their measurement by the proton-transfer-reaction time-of-flight mass spectrometer (PTR-ToF-MS) to reduce the influence of
142 PIDs from other interfering VOCs. A step-by-step procedure for reproducing this method is presented in the Supplement. PIDs
143 were measured by our group and collaborating lab partners by first separating target analytes from a VOC mixture using GC
144 and then measuring the product ions from H_3O^+ ionization (including ionization by impurity reagent ions O_2^+ and NO^+) of the
145 separated VOC using Time-of-Flight Mass Spectrometry (Claflin et al., 2021; Vermeuel et al., 2023). We discuss the details
146 of individual labs' instrument operation below in Section 2.5. Most of the PIDs for the individual VOCs we report here,
147 including measurements from instruments participating in the interlaboratory comparison, were measured from calibration
148 cylinders containing multiple VOCs, while Lab 1 measured some PIDs by sampling an air stream of evaporated liquid VOC
149 solution. VOC sources are listed in the H_3O^+ PID library included as a supplemental document. We found that PIDs were
150 difficult to quantify from VOCs measured from ambient air samples due to the potential influence of coeluting VOCs on the
151 determination of the background subtracted mass spectra. However, because of a lack of calibration standards, we included
152 PIDs measured from ambient samples for ethanol and α -pinene measured by Lab 6 as well as a monoterpene acetate ester
153 measured by Lab 1. Sample concentrations varied depending on cylinder or liquid solution concentrations, but target VOC
154 concentrations were always less than 10 nmol mol^{-1} .

155
156 All the data presented in this manuscript were collected on the "Lab 1" PTR-ToF-MS, unless otherwise noted such as in Section
157 3.2 where we compare PIDs measured from different instruments. We differentiate between the seven different laboratories
158 that contributed data by labelling the data as coming from Labs 1 through 7 (e.g., "Lab 1"). Each instrument used a GC for
159 pre-separation of VOC mixtures and a Vocus Time-of-Flight Mass Spectrometer with H_3O^+ ionization for subsequent
160 measurement of PIDs. In principle, the chemistry discussed here applies to all PTR-MS instruments that use H_3O^+ chemical
161 ionization, but differences in ionization technology, ion transfer optics, and mass analyzers between instruments may have
162 instrument-specific effects on PID measurements. Limited evidence suggests that the PIDs resulting from fragmentation in the
163 Vocus PTR-ToF-MS, as used in this study, and a PTR-MS using a drift tube (instead of an ion-molecule reactor) are
164 comparable (Krechmer et al., 2018), but we limit the implications of our measurements to Vocus PTR-ToF-MS (Tofwerk)
165 instruments until future studies comparing PIDs from different PTR-MS instruments can be performed. The mass spectrometer
166 for Lab 5 used a modified version of the Vocus ionization source (Gkatzelis et al., 2024; Coggon et al., 2024) and the mass
167 spectrometer for Lab 4 had a lower mass resolution compared to the other instruments (approximately 4000 versus 10000 full-
168 width half-maximum, respectively). Lab 5 also used a custom-built GC whereas all the other instruments used a commercially
169 available GC (Aerodyne Research). Because the principle of operation was similar for all instruments, we describe in more



170 detail below the operation of the Lab 1 instrument. Operating details for each of the instruments in the interlaboratory
171 comparison are included in the H₃O⁺ PID library (also outlined in Table 2).

172

173 We describe the GC sampling method used for Lab 1 below but note that operational differences may have been utilized for
174 the different labs represented in the interlaboratory comparison (e.g., temperatures and make-up flow rates). Analytes from
175 multi-component VOC samples were first collected using thermal desorption preconcentration ahead of the chromatographic
176 separation before ionization by the PTR-ToF-MS. For the laboratories that utilized the commercial GC systems, sample air
177 was passed at a rate of 100 cm³ min⁻¹ over a multibed sorbent tube (containing Tenax TA, Graphitized Carbon, and Carboxen
178 1000) where VOCs were collected for 10 minutes. The VOCs were then desorbed from the sorbent tube and collected onto a
179 second preconcentration stage, a focusing trap. VOCs were then rapidly desorbed from the focusing trap and injected on a
180 mid-polarity column (Restek MXT-624, 30 m × 0.25 mm × 1.4 μm). VOCs were separated with a helium carrier gas flow of
181 2 cm³ min⁻¹ during the temperature programmed chromatographic separation. Analyte eluting from the column passed through
182 a transfer line, heated to 100 °C, and was combined with 150 cm³ min⁻¹ of ultra pure zero air before being sampled by the
183 PTR-ToF-MS. Chromatograms were collected over 10 minutes. Versions of the GC system used in this study are described in
184 detail elsewhere (Claflin et al., 2021; Vermeuel et al., 2023; Jensen et al., 2023).

185

186 The PTR-MS sampled the diluted GC eluent/zero air mixture at a rate of 120 cm³ min⁻¹ through a polyether-ether-ketone
187 (PEEK) capillary (25 mm, 0.25 mm ID) which directs the flow to the center of the focusing ion-molecule reactor (IMR). A
188 separate flow of water vapor saturated air enters a pre-chamber where a plasma creates a reagent ion distribution that includes
189 H₃O⁺, water adducts (i.e., H₃O(H₂O)_n⁺ where n = 1,2,3,etc.), as well some amount of O₂⁺ and NO⁺ reagent ions that are
190 considered impurities. These reagent ions from the pre-chamber enter the IMR alongside the eluent sample flow. There are
191 two features of the Vocus PTR-ToF-MS discussed thus far that distinguish this instrument from other instruments that use
192 H₃O⁺ chemical ionization: (1) the Vocus PTR-ToF-MS uses a radio frequency (RF) only quadrupole around the IMR to
193 generate H₃O⁺ ions in excess by declustering water adducts of H₃O⁺ and (2) the water vapor concentration in the IMR is
194 estimated to be approximately 20 % by volume (Krechmer et al., 2018). We do not discuss the effects of IMR quadrupole
195 voltage settings on PIDs here, but instead point the reader to Li et al. (2024) for more information. We do not expect the
196 differences in IMR quadrupole settings utilized in this study to explain the differences observed in the interlaboratory PID
197 comparisons. The higher water vapor concentrations in the Vocus IMR are likely to have impacts that are unique to the Vocus
198 PTR-ToF-MS for PIDs from VOCs historically affected by a water-vapor dependence (e.g., formaldehyde, hydrogen cyanide,
199 and formic acid) compared to PTR-MS instruments using a drift tube where water vapor concentrations are lower.

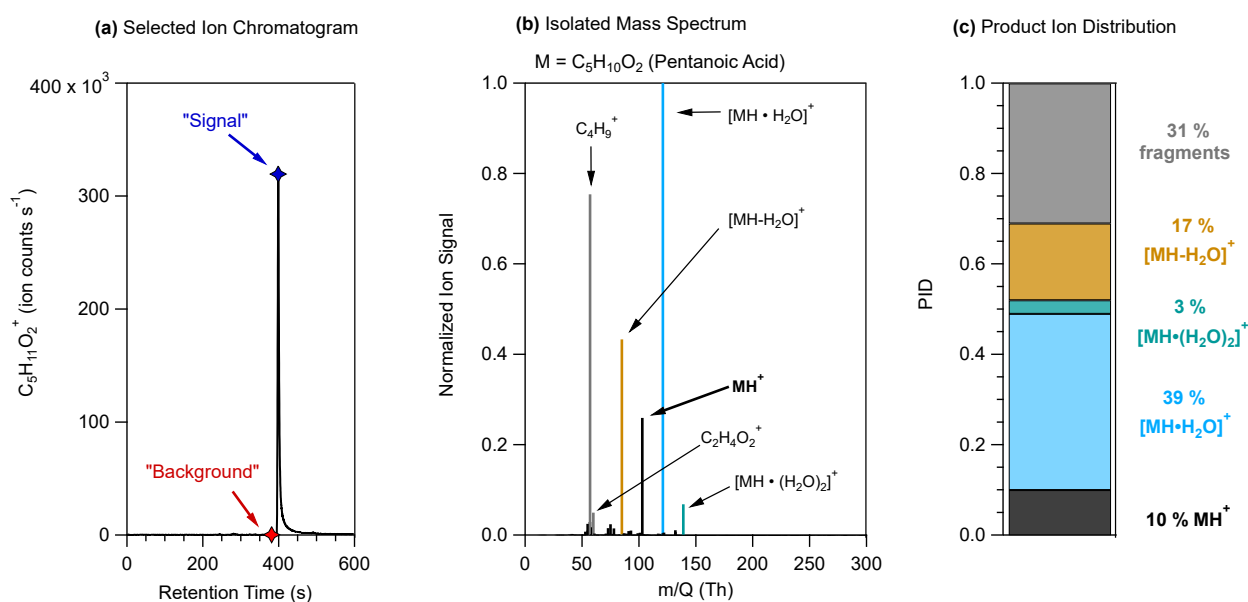
200 2.2.2 PID Quantification from GC-PTR-ToF-MS Measurements

201 For our method of quantifying PIDs, we use chromatographic separation prior to detection of product ions with PTR-ToF-MS.
202 The advantage of using a GC when quantifying PIDs is that analytes in multi-component mixtures (e.g., calibration standards



203 or ambient samples) can be separated before detection and thus avoid interference with PID quantification. Though all the
204 PIDs we present here were determined from GC-PTR-ToF-MS measurements, PIDs can be determined without pre-separation
205 from single component calibration sources. Without pre-separation, multicomponent VOC sources may create product ions
206 that can interfere with quantification of the PIDs from a given VOC.

207 Fig. 1 shows an example, using pentanoic acid, of the chromatographic method of determining PIDs from GC-PTR-ToF-MS
208 measurements.



209
210 **Figure 1: Steps of a method for determining PIDs using pentanoic acid as an example. (a) The selected ion chromatogram for the**
211 **expected H^+ adduct of pentanoic acid, $C_5H_{11}O_2^+$, showing ion signal as a function of retention time. Markers show the retention time**
212 **when the maximum signal (blue) and background (red) mass spectra were defined. (b) The pentanoic acid isolated mass spectrum**
213 **is determined by subtracting the background mass spectrum from the maximum signal mass spectrum. Ion signals are normalized**
214 **to the highest ion signal. (c) Product ion distribution (PID) measured from the isolated mass spectrum for pentanoic acid using data**
215 **from (b).**

216 As shown in Fig. 1a, we use a selected ion chromatogram from the expected H^+ adduct ion signal to determine where to define
217 the background and maximum signal mass spectra. The background mass spectrum is subtracted from the signal mass spectrum
218 to create the isolated mass spectrum shown in Fig. 1b. The high-resolution fitted peak areas of each product ion m/Q , with at
219 least 1 % contribution to the isolated mass spectrum, are added together to represent the sum product ion signal and the relative
220 contribution of each ion to the sum represents the PID. As shown in Figure 1b, some analytes had ions that made small
221 contributions ($< 5\%$) to the isolated mass spectrum in addition to the ions that were included in the PID for pentanoic acid. If
222 ions could not reasonably be explained mechanistically as product ions from the target analyte and made small contributions
223 ($< 5\%$) to the isolated mass spectrum we omitted them in the determination of a PID.



2.3 PID Measurement as a Function of Instrument Settings

In the PTR-ToF-MS instruments in this study, chemistry that forms PIDs occurs in the IMR immediately downstream of the capillary that serves as the sample inlet for the instrument (Fig. 2).

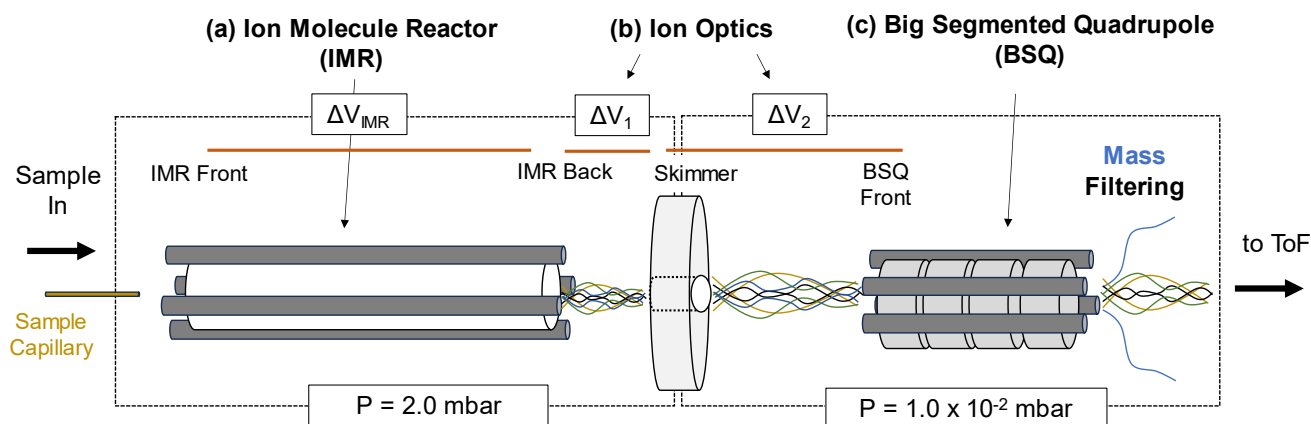


Figure 2: Simplified diagram of the front end of the PTR-ToF-MS evaluated in this study. Sample air enters the instrument through a capillary and is directed to the IMR. (a) The IMR voltage difference between the back and front (ΔV_{IMR}) in part controls the energy of ion collisions. (b) After the IMR, there are two sections of the ion trajectory with voltage differentials that occur at relatively high pressures, these are between the transfer optics (Skimmer – IMR back; ΔV_1 and BSQ front – Skimmer; ΔV_2) as shown. (c) The big segmented quadrupole (BSQ) is an RF-only quadrupole that filters ions acting as a high-pass filter. Pressures for the regions defined by the boxed areas are shown at the bottom of the figure (1 mbar = 100 Pa).

In the IMR a voltage differential (ΔV_{IMR} in Fig. 2) creates an electric field that focuses ions through the reactor. However, the electric field (E , V m^{-1}) strength the ions experience is reduced by the reactor air number density (N , molecules cm^{-3}). The influence of the reduced electric field strength, E/N , on H_3O^+ ion chemistry is well-documented in PTR-MS literature for both drift tube (Yuan et al., 2017) and ion-molecule reactors (Krechmer et al., 2018) and can be calculated following Eq. 1 (De Gouw and Warneke, 2007):

$$\frac{E}{N} = \frac{\Delta V_{\text{IMR}} \cdot T \cdot R}{L_{\text{IMR}} \cdot P \cdot A_v \cdot 10^{-21}} \quad (1)$$

where ΔV_{IMR} is the voltage differential between the IMR back and front (V), T is the IMR temperature (K), R is the ideal gas constant ($8.3 \times 10^{-2} \text{ m}^3 \text{ kPa K}^{-1} \text{ mol}^{-1}$), L_{IMR} is the length of the IMR (10 cm for the instruments in this study), P is the IMR pressure (kPa), A_v is Avogadro's number, and 10^{-21} is a conversion factor from V m^{-2} to the unit of Townsend (Td). We note that for the Vocus instruments discussed here the RF-only quadrupole around the IMR adds to the electric field strength, an effect that is not accounted for in this equation. Li et al. (2024) showed that although the IMR RF voltage can affect analyte sensitivity it did not affect PIDs. All the instruments in this study operated with similar RF voltages for the IMR (between 400 V and 450 V) so we exclude this contribution from the E/N values we report. To measure the effects of E/N on select PIDs in



249 this study, we varied the pressure in the IMR—while keeping the reactor voltage differential (ΔV_{IMR}) constant—between 1.4
250 mbar (0.14 kPa) and 3.0 mbar (0.30 kPa) resulting in E/N values ranging from 90 Td to 190 Td.

251

252 Although PIDs are initially formed in the IMR, m/Q-dependent transmission efficiencies between the IMR and the time-of-
253 flight mass analyzer can affect the PIDs that are ultimately measured (Jensen et al., 2023; Li et al., 2024). We isolate three
254 parts of the ion trajectory in the instrument as possible locations for affecting PIDs through collisional dissociation, quadrupole
255 mass filtering, and/or other transmission effects. The first two areas where ions may undergo declustering of water adducts or
256 collisionally-induced fragmentation are shown in Fig. 2 as ΔV_1 and ΔV_2 , which correspond to the voltage differential between
257 the Skimmer and IMR back (ΔV_1) and the BSQ front and Skimmer (ΔV_2). These ion optic voltage differences have been
258 demonstrated to contribute to declustering reactions in a similar mass spectrometer (Brophy and Farmer, 2016). In this study,
259 we vary the voltage difference between each ion optic component relationship following the methodology of previous studies
260 (Brophy and Farmer, 2016; Lopez-Hilfiker et al., 2016) by incrementally changing the entire set of voltages upstream (i.e., in
261 the direction of the inlet) of the tested component relationship. The range of tested voltages are based on the observed voltage
262 differences in the interlaboratory comparison dataset. For ΔV_1 we measured PIDs as a function of ΔV ranging from -3 V to -
263 50 V and for ΔV_2 we tested a range of -1 V to -10 V.

264

265 The third ion optic component we evaluate is the effect of the RF-amplitude voltage of the big segmented quadrupole (BSQ)
266 in filtering ions of different m/Q. The primary function of the BSQ is to act as a high-pass filter limiting the transmission of
267 lower-mass reagent ions (i.e., H_3O^+ m/Q = 19.02 Th and $(\text{H}_2\text{O})\text{H}_3\text{O}^+$ m/Q = 37.03 Th) to the detector and thus extending the
268 lifetime of the detector (Krechmer et al., 2018). Product ions with an m/Q in the range of these major reagent ions will also
269 experience decreased transmission (Jensen et al., 2023; Li et al., 2024). We measured PIDs at nine different BSQ voltage
270 settings between 225 V and 450 V. Although we focus on three areas where ion m/Q dependent transmission effects may
271 occur, we note that mass discrimination effects can occur elsewhere in the instrument and for other reasons such as detector
272 degradation (Heinritzi et al., 2016) or discrimination of higher m/Q ions because of other quadrupole transmission effects
273 (Holzinger et al., 2019; Antony Joseph et al., 2018).

274 **2.4 PID Measurement as a Function of Sample Capillary Insertion Distance**

275 A small PEEK (25 mm length, 0.18 mm inner diameter) capillary, secured by two Viton o-rings, serves as the sample inlet to
276 the instrument. The distance that this capillary is inserted into the instrument can be manually changed and impacts the
277 ionization chemistry that occurs immediately at the exhausting end of the capillary. We characterized the effects of the capillary
278 insertion distance on the measured PID from pentanoic acid by turning off all voltages to the IMR, closing the standby valve
279 between the IMR region and the rest of the instrument, and manually adjusting the capillary to a different insertion distance.
280 With the capillary at the desired insertion distance we returned the IMR to standard operating conditions and acquired a GC



281 measurement of pentanoic acid. We then changed the capillary insertion distance between 3 mm and 13 mm for five total
282 measurements.

283 **2.5 Interlaboratory Comparison of PIDs**

284 We compare PIDs from seven different instruments under lab-defined settings. Lab-defined settings for all instruments are
285 shown in Table 2.



286
287

Table 2. Lab-defined instrument settings for datasets contributed by each lab. Some labs provided data where the instrument was operated under different settings, and/or data was collected years apart, and thus we differentiate datasets by the letters a, b, and c.

| ID | IMR T (°C) | IMR P (mbar) ³ | ΔV_{IMR} (V) | E/N (Td) | BSQ RF Voltage (V) | ΔV_1 (V) | ΔV_2 (V) | Water Flow (scm ³ min ⁻¹) ⁴ | Inlet Flow (cm ³ min ⁻¹) | Date Acquired |
|-----------------------|------------|---------------------------|----------------------|----------|--------------------|------------------|------------------|---|---|---------------|
| Lab1a | 60 | 2.0 | 580 | 133 | 350 | -22.5 | -4.1 | 20 | 120 | 5/2023 |
| Lab1b | 60 | 2.0 | 580 | 133 | 300 | -22.5 | -4.1 | 20 | 120 | 5/2024 |
| Lab 2a ¹ | 60 | 2.4 | 575 | 110 | 300 | -29.0 | -7.3 | 19 | 100 | 10/2020 |
| Lab 2b ^{1,2} | 60 | 2.4 | 660 | 126 | 400 | -4.4 | -8.1 | 20 | 100 | 11/2023 |
| Lab 3a ² | 100 | 1.5 | 365 | 125 | 215 | -39.7 | -4.5 | 20 | 96 | 12/2020 |
| Lab 3b ² | 100 | 1.5 | 385 | 133 | 215 | -32.0 | -4.0 | 15 | 88 | 11/2022 |
| Lab 4 | 100 | 2.5 | 450 | 122 | 320 | -40.5 | -5.1 | 20 | 79 | 9/2024 |
| Lab 5 ² | 110 | 2.5 | 624 | 131 | 250 | -27.5 | -3.5 | 21 | 180 | 7/2021 |
| Lab 6a ² | 90 | 1.5 | 480 | 160 | 255 | -19.1 | -6.5 | 15 | 260 | 3/2021 |
| Lab 6b ² | 90 | 1.5 | 480 | 160 | 255 | -19.1 | -6.5 | 15 | 290 | 5/2022 |
| Lab 7a | 100 | 2.2 | 570 | 133 | 325 | -39 | -4.2 | 20 | 100 | 4/2022 |
| Lab 7b | 100 | 2.2 | 570 | 133 | 325 | -39 | -4.2 | 20 | 100 | 9/2022 |
| Lab 7c | 100 | 2.2 | 570 | 133 | 325 | -39 | -4.2 | 15 | 100 | 5/2023 |

288 ¹Lab 2a and Lab 2b data comes from two different instruments.

289 ²IMR quadrupole RF voltage was 400 V. The IMR quadrupole RF voltage was 450 V for other instruments.

290 ³1 mbar = 100 Pa.

291 ⁴Standard cm³ min⁻¹ (standard conditions = 293.15 K and 101.325 kPa)

292 2.6 Restroom Air Measurement

293 To demonstrate the uncertainties introduced by PID in ambient air, we deployed our GC-PTR-ToF-MS to a restroom detailed
294 in Link et al. (2024). Briefly, the restroom air sample was acquired during a weekend-long measurement period. The restroom
295 air contained elevated concentrations of terpenoids (i.e., monoterpenes, monoterpene alcohols, and monoterpene acetate esters)



296 that reacted with ozone and created oxygenated VOC products. The relative VOC composition of the restroom air stayed
297 consistent over the measurement period with concentrations decreasing from the start of the period to the end. We highlight
298 one GC chromatogram acquired during that measurement period to demonstrate the effect of PIDs on ion attribution from an
299 indoor air sample.

300 **2.7 Data Processing**

301 During GC measurements mass spectra were collected at a rate of 5 Hz. Mass calibration, resolution and average peak shape
302 determination, and high-resolution peak fitting were all performed in Tofware v3.2.5 (Aerodyne Research). Mass accuracy
303 was maintained within ± 6 ppm when performing mass calibrations. A peak list containing 793 ions was used for high-
304 resolution peak fitting. VOCs present in calibration standards were used to inform what product ions were likely to be expected
305 following the definitions in Table 1. Selected ion chromatograms and isolated mass spectra were produced using the analysis
306 tools in TERN v2.2.20 software (Aerodyne Research).

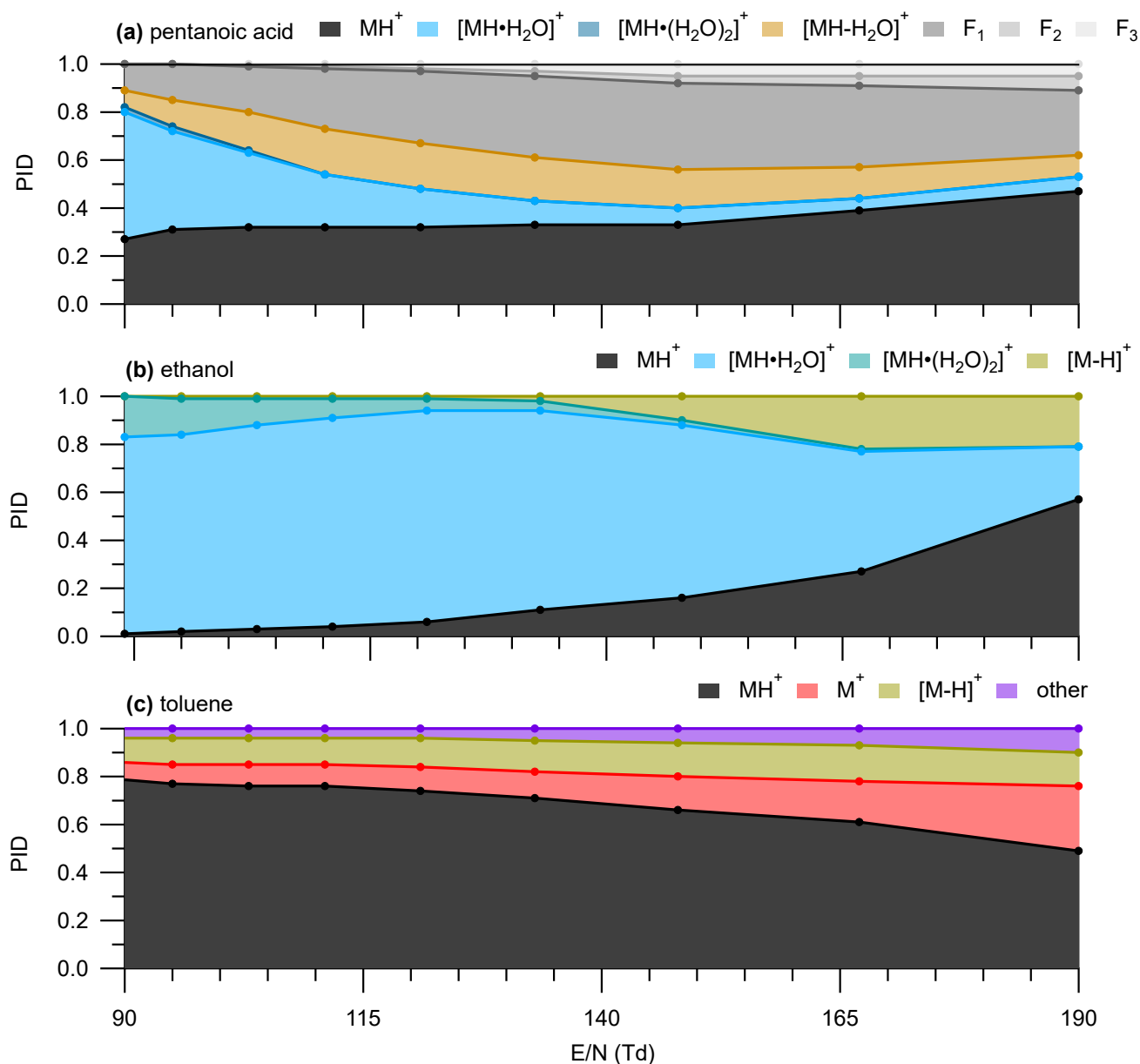
307 **3 Results and Discussion**

308 **3.1 Influence of Instrument Configuration on PIDs**

309 In Section 3.1 we use PIDs measured from pentanoic acid as a case example to describe the influence of instrument settings
310 on PIDs from the Lab 1 instrument. We highlight pentanoic acid because it forms both water clusters and fragments. The
311 formation of cluster and fragment ions from pentanoic acid are dependent on the E/N in the IMR and the m/Q transmission
312 efficiency since the m/Q range of the pentanoic acid PID spans from m/Q 41.04 Th ($C_3H_5^+$, fragment) to m/Q 139.10 Th
313 ($C_5H_{15}O_4^+$, double water cluster) allowing a demonstration of potential mass discrimination effects from the BSQ.

314 **3.1.1 Influence of IMR E/N on PIDs**

315 IMR E/N is an important determinant of water clustering and fragmentation. Fig. 3 shows the PID for pentanoic acid measured
316 at different E/N values.



317

318 **Figure 3: (a) Pentanoic acid PID as a function of E/N. Colored text in the legend above the panel correspond to the colored traces in**
319 **the panel. (b) Ethanol and (c) Toluene as a function of E/N.**

320

321 In the case of pentanoic acid, the contribution of the H^+ adduct increased from 0.26 to 0.47 with increasing E/N (Figure 3).

322 This change in the H^+ adduct contribution was mostly due to the decreasing contribution of the first water cluster from 0.53 at

323 the lowest E/N to 0.06 at the highest E/N. In contrast, the contribution of total fragmentation products (dehydration + other



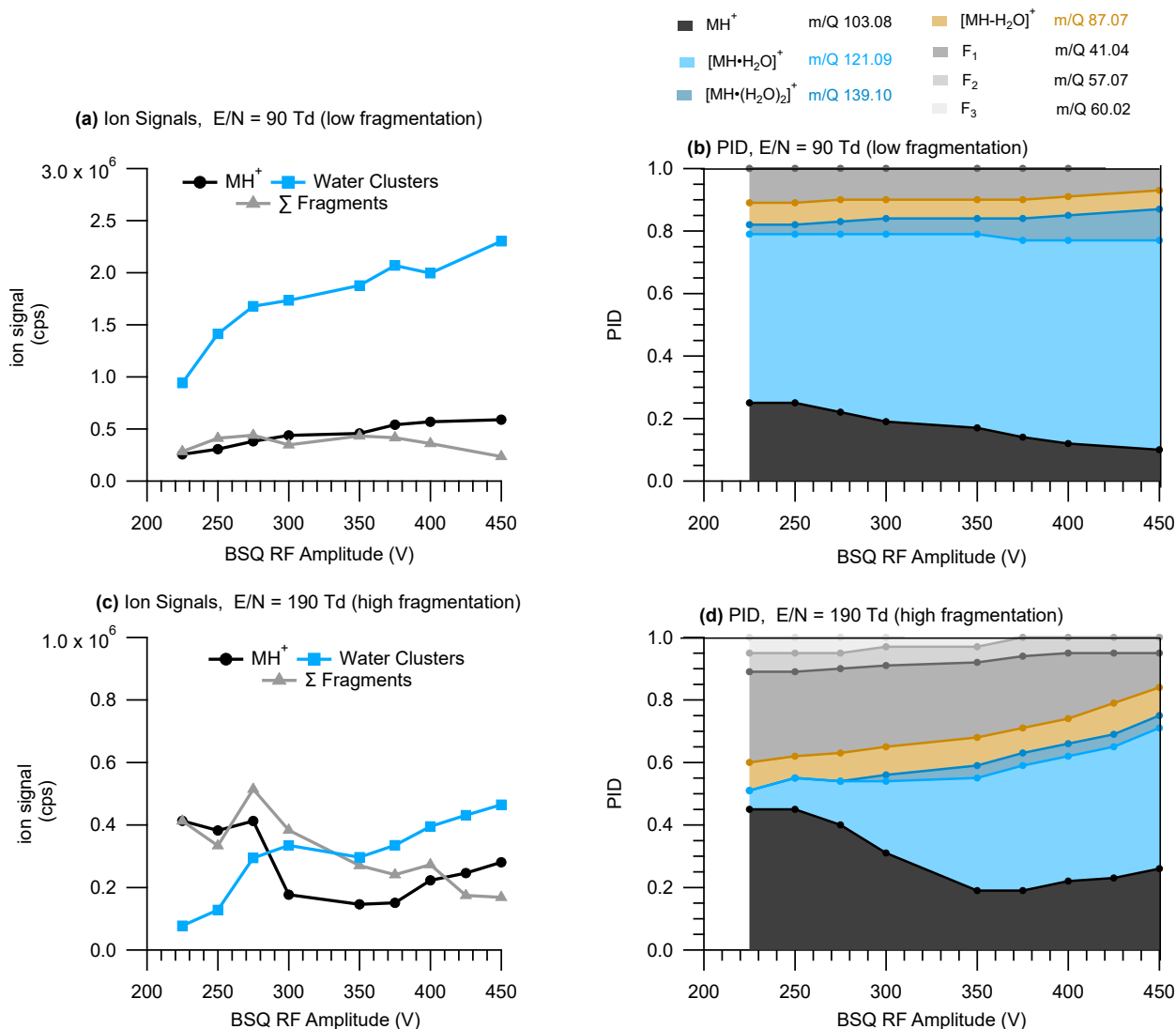
324 fragment ions) increased from 0.20 at the lowest E/N to 0.60 at an E/N of 148 (Figure 3). Above E/N 148, the contribution of
325 the H⁺ adduct to the PID increases and the relative contribution of fragment ions decreases. The general pattern of water cluster
326 and fragment product ion variation with E/N shown in Fig. 3 suggests lower E/N will decrease the contributions fragment ions
327 in the mass spectrum. However, higher E/N values will decrease the contribution of water clusters to the mass spectrum.
328 Because different PIDs (i.e., different contributions of fragments, water clusters, and the H⁺ adduct) are generated at the
329 different values of E/N tested here, measurable product ion formation will likely occur for a variety of VOCs regardless of
330 E/N. As is the case here for pentanoic acid, the secondary product ion is not suppressed across the tested E/N range.

331
332 As another example, we show (Fig. 3b and 3c) how the PIDs vary as a function of E/N for species that can generate product
333 ions from reactions with impurity reagents NO⁺ and O₂⁺. Impurity reagent ions are generated unintentionally in the PTR-ToF-
334 MS and result from oxygen ionizing in the ion source plasma. We show here, using ethanol and toluene as examples, that
335 higher E/N may qualitatively indicate that a user could expect more important contributions of hydride and charge transfer
336 products to the PID. Ethanol forms C₂H₅O⁺, a likely hydride transfer product from reaction with NO⁺, while toluene forms
337 C₇H₇⁺, a likely hydride transfer product from reaction with NO⁺ (Smith et al., 2020), and C₇H₈⁺, a charge transfer product from
338 reaction with both O₂⁺ and NO⁺ (Coggon et al., 2024; Koss et al., 2016). The increased contributions of charge and hydride
339 transfer products to the PIDs of ethanol and toluene potentially suggest an increased influence of impurity reagent ions, but
340 we do not have an explanation for how impurity reagent ion concentrations would increase with increasing E/N in the IMR.
341 We note that the presence of air leaks in the reagent delivery system may increase the importance of impurity reagent ion
342 chemistry. Also, purging the water reagent source with pure nitrogen may be a possible method to mitigate impurity reagent
343 ion chemistry due to the presence of dissolved oxygen.

344 3.1.2 Influence of BSQ RF Voltage on PIDs

345 Another important influence on PIDs from pentanoic acid was the BSQ RF amplitude voltage (referred to hereafter as “BSQ
346 voltage”). BSQ voltages observed from the lab-defined settings in the interlaboratory comparison dataset ranged from 215 V
347 to 400 V. The BSQ acts as a high-pass filter and thus low-mass ion transmission decreases with increasing BSQ voltage. In
348 other words, at low BSQ voltages (e.g., 225 V) we would expect to see greater transmission of low-mass ions (e.g., m/Q <
349 55.04 Th) compared to higher voltages (e.g., 450 V). When considering how the BSQ affects PIDs we expected that product
350 ions that were low-mass, both H⁺ adduct and fragment ions, would be most affected by different BSQ voltages versus the
351 higher m/Q water cluster products.

352
353 Fig. 4 shows the ion signals and PIDs for pentanoic acid measured across a range of BSQ voltages under two extreme IMR
354 E/N conditions—high clustering/low fragmentation (i.e., lower E/N, 90 Td) and low clustering/high fragmentation (i.e., higher
355 E/N, 190 Td).



356

357 **Figure 4: Pentanoic acid product ion signals (a and c) and PIDs (b and d) as a function of BSQ RF Amplitude voltage measured with**
 358 **IMR (a and b) E/N = 90 Td, corresponding to “higher clustering/lower fragmentation” conditions and (c and d) E/N = 190 Td,**
 359 **corresponding to “lower clustering/higher fragmentation” conditions. (a and c) The ion signals for the MH⁺ ion, sum of the water**
 360 **cluster product ions, and sum of the fragment product ions were determined by integrating product ion peaks from their selected**
 361 **ion chromatograms.**
 362

363 The ion signals in Fig. 4 demonstrate the effect of the BSQ voltage on total transmission of ions whereas the PIDs demonstrate
 364 transmission effects relative to other ions. For instance, when E/N was 90 Td, the H⁺ adduct ion signal increased with increasing
 365 BSQ voltage (Fig. 4a), but the relative contribution of the H⁺ adduct to the PID decreased (Fig. 4b). Because the water cluster
 366 ion signals were increasing more than the H⁺ adduct as BSQ voltage increased, the relative contribution of the water cluster



367 ion signals to the PID increased. In contrast, the sum of the ion signals for fragments, under both E/N conditions, decreases
368 with increasing voltage because of the decreased transmission efficiency of the lower m/Q ions.

369
370 BSQ effects on PIDs are likely to be most pronounced for VOCs that generate lower m/Q ions like the fragment ions generated
371 from pentanoic acid. The contribution of fragment ions to the PID for pentanoic acid are most pronounced when the IMR E/N
372 is 190 Td and water cluster contributions are low relative to when the IMR E/N was 90 Td. As the BSQ voltage increases, the
373 lowest m/Q product ion ($C_3H_5^+$, $C_4H_9^+$, and $C_2H_4O_2^+$) contributions decrease at an E/N of 190 Td. At 450 V the $C_2H_4O_2^+$ ion
374 is no longer making measurable contributions to the PID and the contribution of $C_4H_9^+$ has decreased by a factor of five.
375 However, as the contribution of lower m/Q ions to the PID decreases with increasing BSQ voltage the contribution of higher
376 m/Q ions (H^+ adduct and water clusters) generally increase for pentanoic acid. Notably, the relative contribution of the single
377 water cluster to the PID, when E/N = 190 Td, increases by a factor of eight at 450 V compared to 225 V.

378 3.1.3 Influence of Ion Optic Voltages and Capillary Distance on PIDs

379 We found that ion optic voltage differences (i.e., ΔV_1 and ΔV_2) and the capillary insertion distance did not impact the pentanoic
380 acid PID as clearly as E/N and the BSQ settings. Figures presented in the Supplement demonstrate the variability in PIDs
381 measured for pentanoic acid when testing the voltage differences for ΔV_1 (Fig. S1) and ΔV_2 (Fig. S2), and the sample capillary
382 insertion distance (Fig. S3). We also analyzed the PID for benzene to investigate if charge transfer product ions were modulated
383 by the capillary distance.

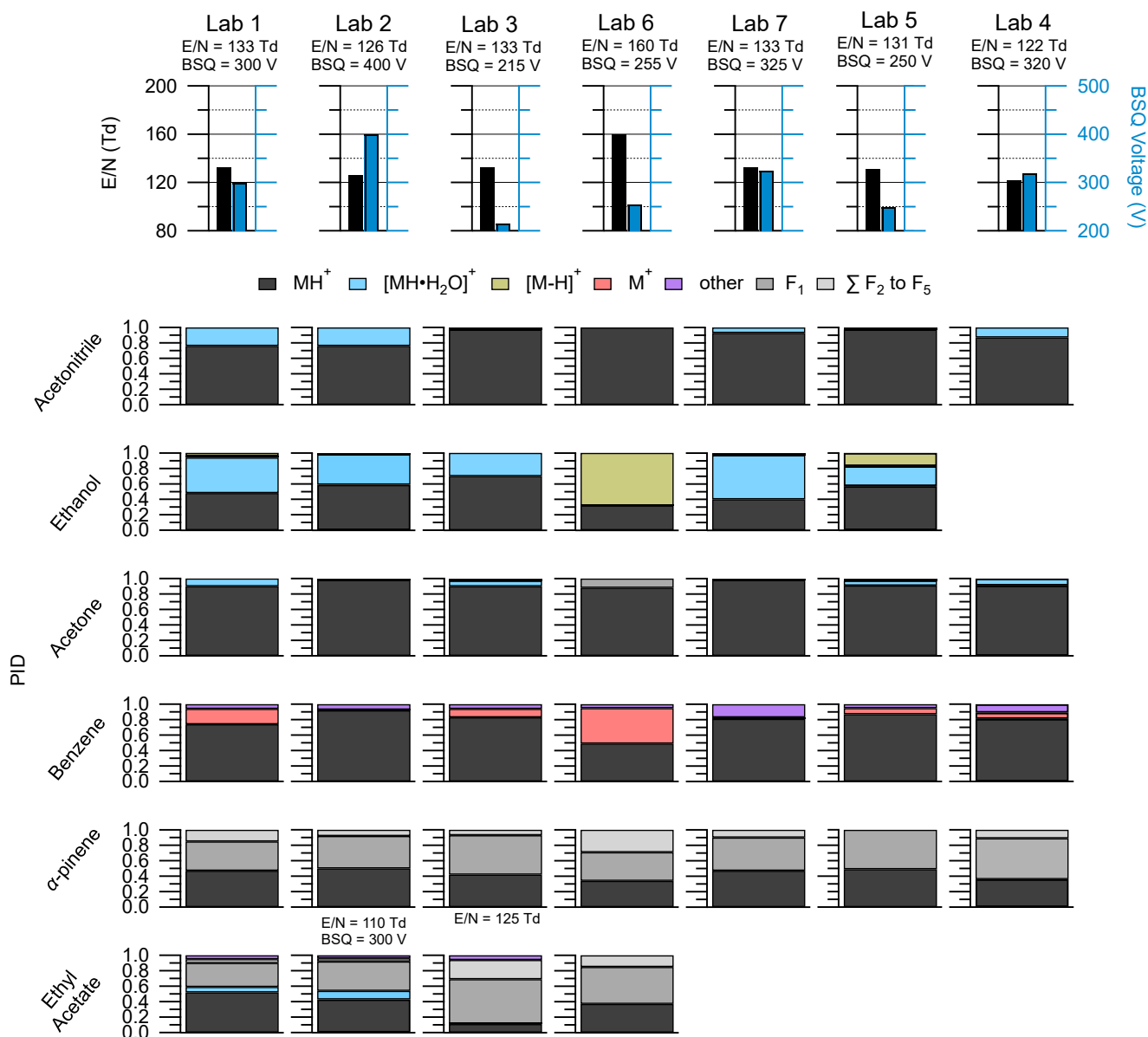
384
385 We did not observe any clear trends in PID variability as a function of both tested ion optic voltage differences (Fig. S1 and
386 Fig. S2). We also did not observe any clear trends in the PID for pentanoic acid or the charge transfer product ion contributions
387 to the benzene PID as a function of capillary distance. We conclude that E/N and BSQ voltages mostly drive variability in
388 PIDs, and the other ion optic and capillary distance configurations tested here impact PIDs to a lesser extent.

389 3.2 Interlaboratory Comparison of PIDs

390 We compare PIDs measured from the seven laboratories under lab-defined settings. Acetonitrile and α -pinene were the only
391 VOCs with PIDs measured by every lab. We highlight select VOCs with a particular propensity for water cluster and/or
392 fragment ion formation, that were commonly measured amongst the labs, for a qualitative comparison. We then compare a
393 more diverse suite of VOCs for a quantitative characterization of PIDs across instruments.

394 3.2.1 Qualitative Comparison of PIDs Across Instruments

395 Figure 5 highlights differences in PIDs measured from select VOCs common across most of the instruments.



396

397 **Figure 5: The top row shows the lab identity label (i.e., Lab 1, Lab 2, etc.) and corresponding E/N (left axis) and BSQ voltages (right**
 398 **axis; blue) used for the PID measurements shown below. PIDs measured for select VOCs from the interlaboratory comparison**
 399 **dataset. Empty spots where a barplot would be indicate that lab did not have measurements for the VOC in the corresponding row.**
 400 **The PIDs for ethyl acetate were measured for Lab 2 and Lab 3 under slightly different instrumental conditions than the rest of the**
 401 **VOCs and the corresponding E/N and BSQ voltages are shown above the barplots. Contributions of 3 % or less to the PID may be**
 402 **difficult to see in the figure, but exact values can be found in the H₃O⁺ PID library.**
 403



404 Data shown in Fig. 5 originate from instruments operating within a relatively narrow range of E/N (122 Td to 133 Td) with
405 the exceptions of Lab 6 which ran at an E/N of 160 Td and the ethyl acetate measurement from Lab 2. Our analyses of pentanoic
406 acid PID variability as a function of instrument configuration provide some context for interpreting the PID variability observed
407 here. Measurements of the pentanoic acid PID as a function of E/N in Fig. 3 demonstrate that variability in water cluster and
408 fragment product ion contributions to the PID may vary on the order of approximately 10 % when comparing measurements
409 acquired at an E/N of 120 Td versus 130 Td.

410

411 The appearance and contribution of product ions to the PID of a given VOC varied between instruments and was not always
412 easily explained by variations in E/N and/or BSQ voltage. Water clusters made some contribution to the PID from at least one
413 of the VOCs for each lab except Lab 6 which operated at the highest E/N (160 Td). However, the contribution of the water
414 cluster to the PID for acetonitrile was 24 % for Lab 1 and 3 % for Lab 7 despite operating with nearly the same E/N and BSQ
415 voltage. We expected the acetone PID could provide evidence of BSQ low-mass filtering as the m/Q of the H⁺ adduct ion (m/Q
416 59.05 Th) is lower than the water cluster product ion (m/Q 77.06 Th) and so lower BSQ voltages may correspond to higher
417 contributions of the H⁺ ion to the PID compared to the water cluster. Comparison of the acetone PID from Lab 1 versus Lab 2
418 and Lab 7 displays the opposite trend where, when BSQ voltage increases, the contribution of the H⁺ ion increases compared
419 to the water cluster ion. This comparison of the acetone PID with BSQ voltage demonstrates the challenge of generalizing
420 patterns of PIDs from a single instrument setting.

421

422 Each instrument in this intercomparison was operated with a different BSQ voltage which likely influenced variability in PIDs
423 between instruments. For several of the VOCs in Fig. 5 we might expect higher contributions of water clusters to the PIDs for
424 acetonitrile, ethanol, and acetone at higher BSQ voltages because higher voltages decrease the transmission efficiency, relative
425 to water clusters, for the H⁺ adduct. For instance, Lab 3 operated with a BSQ voltage of 215 V and Lab 2 operated with a
426 voltage of 400 V representing the lower and upper ends, respectively, of the dataset BSQ voltage range. One possible
427 explanation for the difference in the water cluster contribution to the acetonitrile PID, measured for Lab 3 and Lab 2 of 3 %
428 and 24 % respectively, is increased relative transmission efficiency of the water cluster at the higher BSQ voltage used in Lab
429 2 (both labs have similar E/N).

430

431 Ethyl acetate was also impacted by BSQ voltage effects (Fig. 5). The E/N for the Lab 3 (E/N = 122 Td) measurement of ethyl
432 acetate falls in between that of Lab 1 (E/N = 133 Td) and Lab 2 (E/N = 110 Td) and thus we might expect the PID to be similar
433 to those two labs. In contrast to Labs 1 and 2, the Lab 3 ethyl acetate PID shows a higher contribution of fragment ions and
434 does not show a water cluster contribution. The two major fragment ions for ethyl acetate (C₂H₃O⁺ = 43.02 Th and C₂H₅O₂⁺ =
435 61.03 Th) are similar in m/Q to the fragment ions of pentanoic acid (C₃H₅⁺ = 41.04 Th and C₄H₉⁺ = 57.07 Th) that we saw
436 affected by the BSQ voltage in Fig. 4. Thus, the lower BSQ voltage used for Lab 3 (BSQ = 215 V), compared to Labs 1 (BSQ



437 = 300 V) and 2 (BSQ = 400 V), likely increased the transmission efficiency of fragment ions, relative to the H⁺ adduct and
438 water cluster, and increased their contribution to the PID for Lab 3.

439

440 Of the VOCs presented here, α -pinene, shows considerable fragmentation, but also reasonable agreement in the PID ($\pm 10\%$
441 for any given product ion contribution to the PID) across instruments. Variability in α -pinene PIDs between instruments can
442 be qualitatively explained by differences in E/N. Lab 6, operating at an E/N of 160 Td (higher fragmentation than the other
443 instruments), showed a near equal contribution of the H⁺ adduct, F₁, and sum of other fragments to the PID whereas the other
444 instruments showed roughly half H⁺ adduct, half F₁, with some (< 10%) contribution of the sum of other fragments. We expect
445 α -pinene, and most other monoterpenes, to be minimally influenced by changes in BSQ voltage (and thus low-mass filtering
446 effects) as most of the major product ions are greater than m/Q 55.04 Th (corresponding to the reagent ion double water cluster,
447 (H₂O)₂H₃O⁺) where mass-filtering effects are expected to be less pronounced (Krechmer et al., 2018).

448

449 Reagent ion impurities, O₂⁺ and NO⁺, are likely responsible for charge and hydride transfer product ions observed for benzene
450 and ethanol shown in Fig. 5. In Fig. 3 we show that the PID contribution for both hydride (as seen for ethanol and toluene) and
451 charge transfer products (as seen for toluene) increase with increasing E/N. However, variability in E/N does not explain the
452 differences in hydride transfer product contributions to the PID for ethanol and charge transfer product contributions to the
453 PID for benzene between the labs in Fig. 5. Lab 6, which operated with the highest E/N (160 Td), had the largest contributions
454 of both the hydride transfer product for ethanol and the charge transfer product for benzene which is consistent with the
455 observation of more impurity reagent ion chemistry at higher E/N. However, Lab 1 and Lab 7 operated with nearly the same
456 E/N and BSQ voltage, but Lab 7 did not measure the charge transfer product for benzene whereas Lab 1 measured a 20%
457 contribution. We hypothesize that increased inlet flow rates increase O₂⁺ and/or NO⁺ chemistry as evidenced by the ethanol
458 hydride transfer product making the largest contributions to the ethanol PID for Lab 5 and Lab 6 which operated their
459 instruments at higher flowrates compared to the other labs (Lab 5 = 180 cm³ min⁻¹ and Lab 6 = 290 cm³ min⁻¹, while the other
460 systems operated with an inlet flow rate of approximately 100 cm³ min⁻¹).

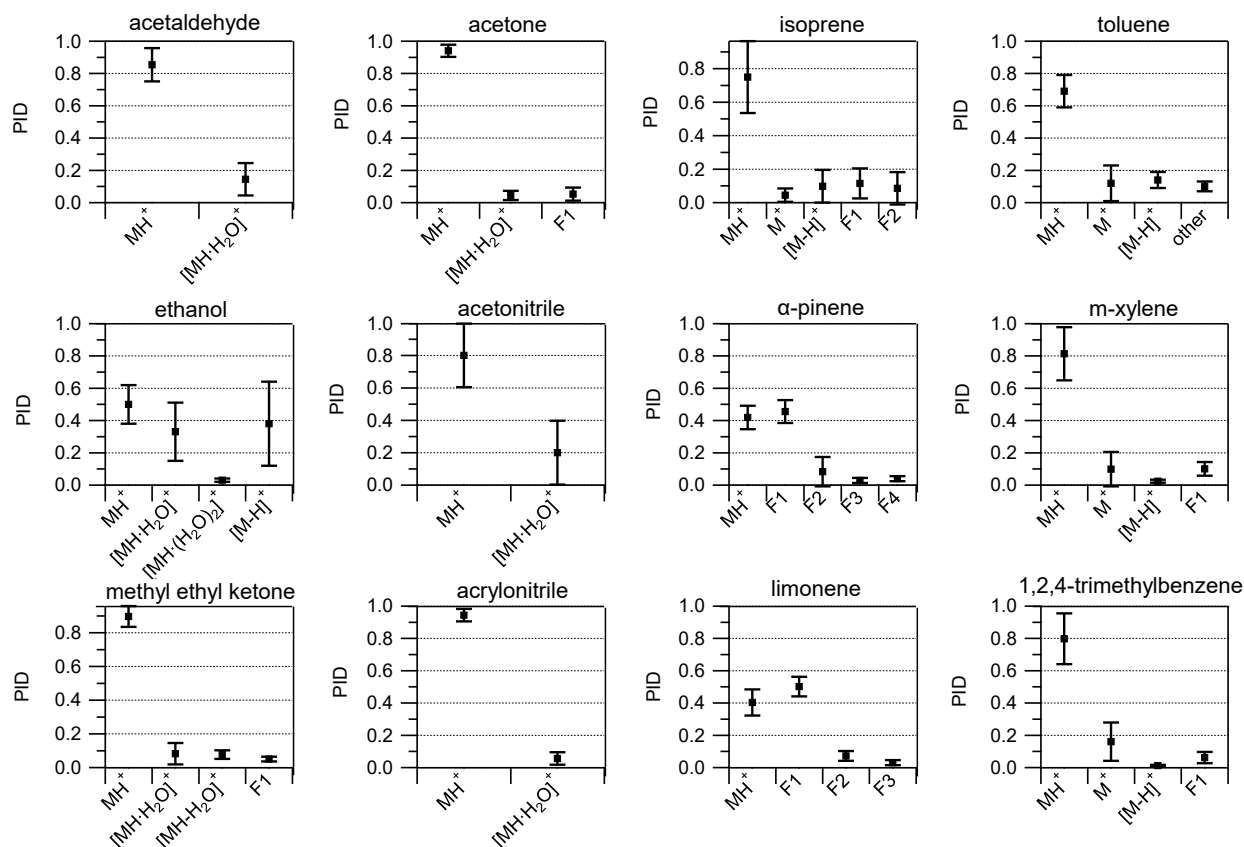
461

462 We note that several aromatics (e.g., benzene, toluene, chlorobenzene) also generated a product ion, C₆H₇O⁺, that we could
463 not identify a mechanism for and we classified as “other”. With regard to benzene detection, this product ion contributed 20
464 % to the PID for Lab 7 but made smaller contributions (< 5%) to the PIDs for other labs. In the case of Lab 7, larger
465 contributions of C₆H₇O⁺ did not coincide with enhanced contributions of the charge transfer product to the benzene PID so
466 this ion may not be a product of O₂⁺ and/or NO⁺ chemistry. Because C₆H₇O⁺ is generated from several aromatics (see H₃O⁺
467 PID library) it may be an important isobaric interference for phenol.



468 **3.2.2 Quantitative Comparison of PIDs Across Instruments**

469 We calculated the average and standard deviation of the mean of the product ion contributions to the PIDs for 12 VOCs
 470 contained within the interlaboratory comparison dataset (Fig. 6).



471
 472 **Figure 6: Averages (black squares) and standard deviations of the mean (1 σ) of PIDs for select VOCs. Averages were determined**
 473 **from at least five measurements from the interlaboratory comparison dataset. The number of individual measurements used to**
 474 **calculate average and standard deviation values can be found in Table S1.**

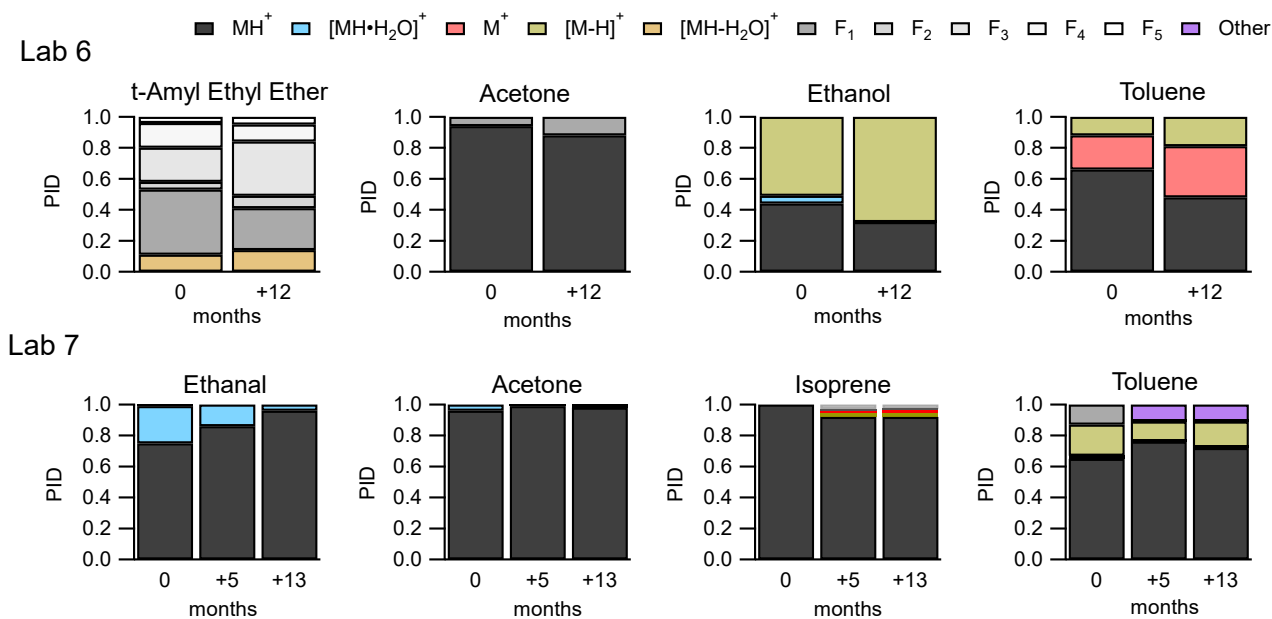
475
 476 Many of the VOCs had standard deviations (1 σ) associated with product ions that varied no more than 20 % thus providing a
 477 constraint for predicting PIDs across instruments operating under different conditions. This relatively tight distribution of
 478 product ion abundance also suggests the H₃O⁺ PID library included as a supplemental spreadsheet could be a useful guide for
 479 estimating PIDs from Vocus PTR-ToF-MS instruments. Ethanol and acetonitrile showed considerable (i.e., > 40 %) product
 480 ion variability (Fig. 6). For ethanol, the importance of the water cluster was highly dependent on E/N. Additionally, the fraction
 481 of the hydride transfer product ranged from < 5 % to roughly 50 %. The ethanol and acetonitrile PIDs are not only influenced
 482 by E/N but also likely impacted by the BSQ voltage since the H⁺ adducts are a relatively low m/Q (i.e. m/Q < 55.04 Th). VOCs



483 like isoprene and the aromatics have PIDs that are impacted by NO^+ and O_2^+ reagent ion chemistry which, as discussed above,
 484 is difficult to predict without directly measuring PIDs of susceptible VOCs. Although E/N influences PIDs, the general trend
 485 of fragmentation/declustering with increasing E/N can be used as a guideline to inform a user how they might expect their
 486 PIDs to deviate from the averages shown in Fig. 6.

487 3.2.3 Consistency of PIDs Measured Over Time

488 Two labs, Lab 6 and Lab 7, provided data where the instrument was operated under the same voltage configurations, but PIDs
 489 were measured a year or more apart. Figure 7 shows the variability in PIDs for four select VOCs from these two labs over a
 490 year.



491
 492 **Figure 7: PIDs for select VOCs from Lab 6 (top frames) and Lab 7 (bottom frames) showing variability of PIDs over one year.**

493
 494 Measurements from both labs indicate that, given the same voltage configurations on the same instrument, PIDs can change
 495 over time. The largest change from the subset of VOCs in Fig. 7 is the water cluster contribution to the ethanal (acetaldehyde)
 496 PID, from Lab 7, starting at 24 % and decreasing to 4 % after 13 months. Toluene, measured from Lab 7, has a fragment
 497 product ion starting out that is no longer detected after five months and instead the product ion $\text{C}_6\text{H}_7\text{O}^+$ begins to make
 498 contributions to the PID. Similarly, isoprene from Lab 7 has fragment and charge/hydride transfer product ions that appear in
 499 the PID after five months.

500



501 The PIDs for the four VOCs from Lab 6 show greater contributions of fragment and charge/hydrate transfer product ions after
502 12 months compared to the first measurement. We hypothesize three possible factors could be related specifically to the
503 increase in charge/hydrate transfer product ions over time: (1) the increase in inlet flowrate ($260 \text{ cm}^3 \text{ min}^{-1}$ at 0 months to 290
504 $\text{cm}^3 \text{ min}^{-1}$ at +12 months), (2) capillary insertion depth, and (3) leaks into the sampling system from maintenance. Lab 6 reports
505 that after maintenance on their instrument changes in instrument performance (e.g., sensitivity) were observed and may be
506 associated with cleaning the capillary that serves as the inlet to the instrument (Jensen et al., 2023). The instrument was in a
507 stable condition after maintenance before the PIDs were collected. Although we did not observe a strong dependence of NO^+
508 and O_2^+ chemistry on capillary insertion distance for the Lab 1 instrument (Fig. S3), it is possible that at the higher inlet
509 flowrates, used for the Lab 6 measurements, an effect could be observed.

510

511 None of the product ions from this example change their contribution to the PID by more than 10 % over time—with the
512 exception of the ethanal water cluster. This time-dependent variability in PIDs demonstrated in Fig. 7 points to some factor or
513 combination of factors affecting PIDs not considered in our analyses (e.g., degradation of the microchannel plate detector
514 (Müller et al., 2014)). Additionally, the variability of individual product ions over time provides an estimate of natural
515 variability on the order of 10 % (but as high as 20 %) when comparing product ion contributions to PIDs between instruments
516 like we did in Section 3.2.1.

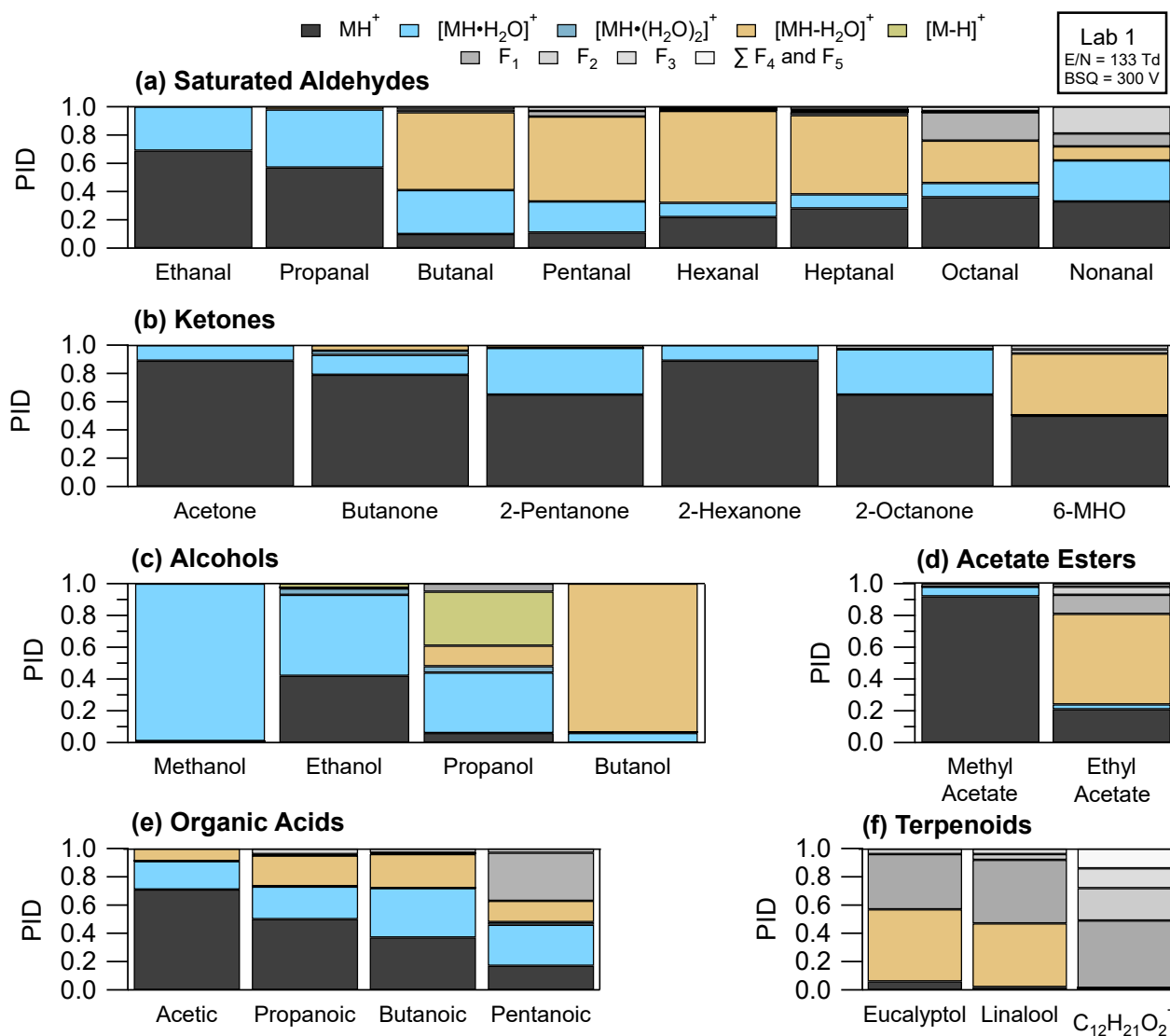
517 **3.3 Measurements of PIDs for Oxygenated VOCs from Lab 1**

518 We highlight features of PID formation from VOCs with oxygenated functionalities that may be measured in high
519 concentrations from samples of indoor air and/or urban air plumes in the sections below. Product ion formation is characterized
520 in the literature for some VOCs like aromatics and monoterpenes (Yuan et al., 2017; Misztal et al., 2012; Materić et al., 2017)
521 that do not readily form water clusters. Product ion formation from oxygenated VOCs is less well-characterized, particularly
522 for water cluster formation.

523

524 Figure 8 shows PIDs for select VOCs categorized by functional group as measured from Lab 1 using calibration standards
525 (except for the unidentified monoterpene acetate ester which was measured from a restroom air sample). PIDs were measured
526 under instrument settings that correspond to Lab 1b in Table 1. A key result demonstrated in Fig. 8 is that, for the subset of
527 VOCs shown here, the H^+ adduct contribution to the PID is often less than 60 % and thus air samples containing these VOCs
528 may have many product ions populating the mass spectra. In other words, H_3O^+ ionization is generating unintended product
529 ions often at similar rates as the intended H^+ adduct for most VOCs. Below we discuss general patterns of product ion formation
530 from VOCs with varying functionalities.

531



532

533 **Figure 8: PIDs measured for Lab 1 for select VOCs representing different functional groups. VOCs from left to right, per functional**
 534 **group, are in order of increasing carbon number. “ $C_{12}H_{21}O_2^+$ ” is an unidentified monoterpene acetate ester, measured from a**
 535 **restroom air sample, likely originating from isobornyl or linalyl acetate.**

536 3.3.1 Saturated Aldehydes

537 Recently, fragment product ions from saturated aldehydes have been highlighted in measurements of urban air influenced by
 538 cooking emissions (Coggon et al., 2024), ozonolysis of sea water (Kilgour et al., 2024), and ozonolysis products of human
 539 skin oils in indoor air (Wang et al., 2024; Ernle et al., 2023). In the Lab 1 instrument fragment product ions contributed > 40
 540 % to the PID for saturated aldehydes with a carbon number greater than three (i.e., butanal to nonanal). Water cluster formation
 541 contributed > 20 % to the PID for ethanal (acetaldehyde), propanal, and nonanal. As reported previously for butanal through



542 heptanal (Buhr et al., 2002), the fragment ion making the largest contribution to the PID in the Lab 1 instrument was the
543 dehydration product (i.e., $[MH-H_2O]^+$). We find additional agreement with previous literature reporting octanal and nonanal
544 fragmentation to smaller product ions (e.g., $C_5H_9^+$, $C_3H_5^+$, $C_6H_{11}^+$). We suspect, from limited experimental data (Španěl et al.,
545 2002), that larger saturated aldehydes (e.g., decanal) may also produce fragment product ions smaller than the dehydration
546 product ion in the Lab 1 instrument. However, as the carbon number of the saturated aldehyde increases, from butanal, the
547 contribution of the H^+ adduct to the PID increases—and the contribution of dehydration and fragment product ions decrease—
548 suggesting larger aldehydes fragment less overall than butanal, pentanal, and hexanal.

549 3.3.2 Ketones

550 In contrast to saturated aldehydes, and consistent with previous work (Buhr et al., 2002), the saturated ketones (i.e., all the
551 ketones in Fig. 8b except 6-MHO) measured with the Lab 1 instrument do not fragment substantially (i.e., sum of fragment
552 contributions to PID < 5 %). However, the saturated ketones do form water clusters with contributions ranging from 10 %
553 (e.g., acetone) to 40 % (e.g., 2-octanone) to the PID. We do not observe a clear relationship between increasing carbon number
554 and water clustering. In fact, when comparing 6-methyl-5-heptan-2-one (6-MHO) and 2-octanone, two eight carbon molecules,
555 the water cluster for 2-octanone contributed 40 % to the PID whereas 6-MHO had no detectable water cluster formation (Fig.
556 8b). Additionally, as demonstrated by the PID from 6-MHO, adding carbon branching and/or additional functionalities can
557 change product ion formation considerably compared to the saturated C_8 ketone analogue.

558 3.3.3 Alcohols

559 We observed important contributions of water clusters (> 40 %) to the PIDs measured for methanol, ethanol, and propanol.
560 Methanol and ethanol can be present in concentrations that exceed 1 nmol mol^{-1} in both outdoor and indoor air and thus the
561 water clusters of these two alcohols may make important contributions to sample mass spectra. We also measured small
562 contributions of double water clusters to the PID from ethanol and propanol (4 % for each VOC). Previous studies have shown
563 considerable fragment product ion production from dehydration of alcohols (Buhr et al., 2002; Španěl et al., 2002; Warneke
564 et al., 2003; Pagonis et al., 2019) and we also observed that for propanol and butanol. For butanol > 90 % of the PID was from
565 the dehydration product ion and we did not measure any generation of the H^+ adduct. We also observe small contributions of
566 the hydride transfer product from ethanol that have been reported from another PTR-ToF-MS (Coggon et al., 2024) and
567 measured with the NO^+ reagent from a selected ion flow tube study (Španěl et al., 2002). The hydride transfer product made a
568 30 % contribution to the PID measured for propanol. As summarized in Koss et al. (2016), several other saturated alcohols
569 have hydride transfer enthalpies that decrease with increasing carbon number and thus hydride transfer product ions may
570 appear in PTR-MS spectra from ambient air samples where saturated alcohols may be in high abundance. As an example,
571 Buhr, et al. (2002) measured 10 % contribution of the hydride transfer product from 1-octanol and 2-octanol to their PIDs.

572



573 Although we focus on reaction with NO^+ as the primary reagent producing hydride transfer products from reaction with VOCs,
574 Hegen et al. (2023) hypothesized that charge transfer from O_2^+ to methanol, with subsequent loss of hydrogen atom, may be
575 an important mechanism for creating product ions that appear in the mass spectrum as hydride transfer products. Thus, both
576 charge and hydride transfer enthalpies may be useful qualitative indicators for predicting if $[\text{M-H}]^+$ product ions are generated
577 from ionization of alcohols. For VOCs whose PIDs are not included in the H_3O^+ PID library, we refer the reader to Koss et al.
578 (2016) for a table of hydride and charge transfer enthalpies for many VOCs measured using PTR-MS as a useful resource for
579 predicting the possible generation of product ions.

580 3.3.4 Acetate Esters, Organic Acids, and Oxygenated Monoterpenes

581 Neither the acetate esters nor oxygenated monoterpenes in this study show a propensity to form water clusters. We measure
582 considerable fragmentation of ethyl acetate (Fig. 8d). In addition to ethyl acetate, Buhr et al. (2002) measured major
583 contributions of fragmentation products of several other acetate esters to their PIDs. Although Buhr et al. (2002) used an older
584 model of PTR-MS with a drift tube ionization region, we expect that larger acetate esters may also fragment to the same degree
585 as observed in that study in the Vocus PTR-ToF-MS.

586
587 Alkanoic acids have PIDs that show complexity similar to the saturated aldehydes with extensive water cluster formation and
588 fragmentation (Fig. 8e). Notably, the fraction of H^+ adduct in the PID decreases with increasing carbon number with roughly
589 15 % of the PID for pentanoic acid allocated to the H^+ adduct. More data is needed, but this trend suggests larger organic acids
590 (i.e. $> \text{C}_5$) may also produce water cluster and fragment product ions in similar abundance to the H^+ adduct. Characterization
591 of PIDs for larger (e.g., C_9 and C_{10}) acids may be of particular importance for measurements of early generation oxidation
592 products of terpenes.

593
594 Notably, the contribution of the H^+ adduct to the PID for the terpenoids highlighted here are all less than 5 %. The monoterpene
595 alcohols (eucalyptol and linalool) generate dehydration product ions with abundances greater than 40 % (Fig. 8f). The
596 dehydration product of the monoterpene alcohols, $\text{C}_{10}\text{H}_{17}^+$, is isobaric (i.e., occurring at the same m/Q) with the H^+ adduct for
597 monoterpenes. We also highlight the PID measured for $\text{C}_{12}\text{H}_{21}\text{O}_2^+$, a monoterpene acetate ester (most likely linalyl or isobornyl
598 acetate based on offline GC analysis presented in Link, et al. (2024)), measured from a restroom air sample. This ion fragments,
599 losing a neutral acetic acid, to form $\text{C}_{10}\text{H}_{17}^+$ suggesting monoterpene acetate esters may also create monoterpene interferences
600 from samples where monoterpenes and the acetate esters are both present.

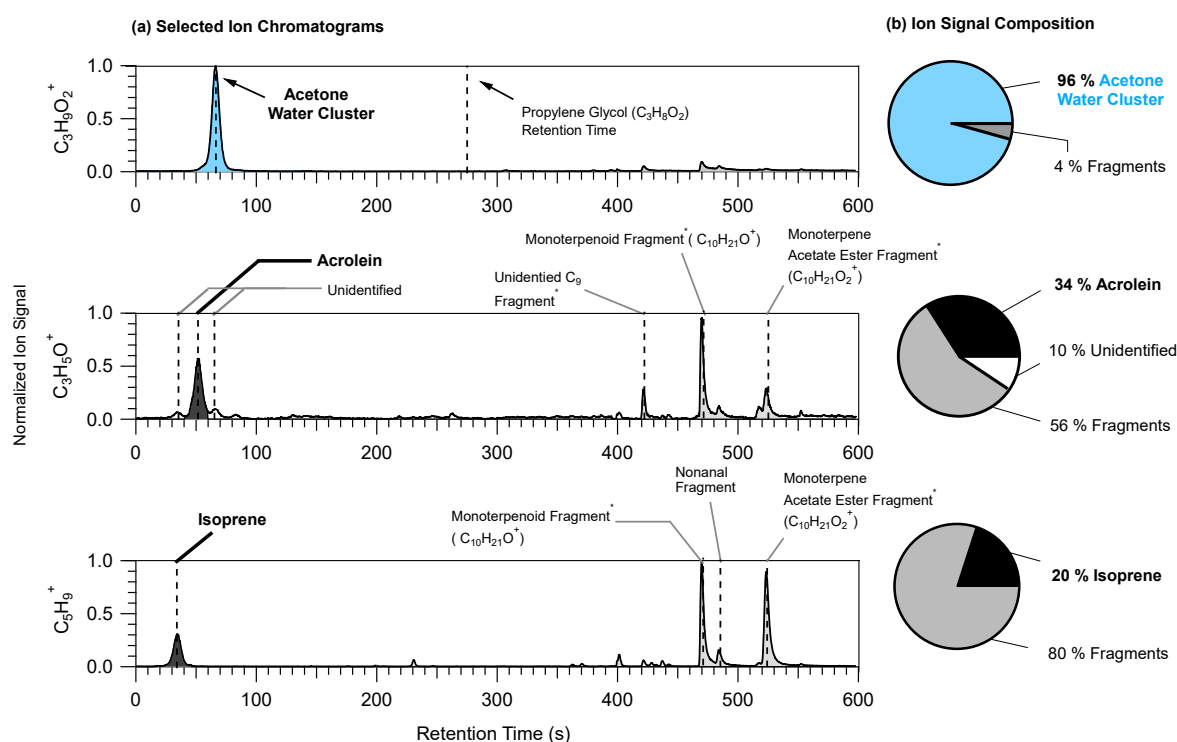
601 3.4 Mass Spectral Ambiguity from the Influence of PIDs: A Restroom Air Sample Case Study

602 One consequence of multi-product ion generation in PTR-MS is that if PIDs are unknown or uncharacterized they can create
603 ambiguity when identifying peaks in the mass spectrum in the absence of a pre-separation method. In particular, studies
604 performing non-targeted analysis of the ion signals measured by PTR-MS from indoor air samples (Link et al., 2024; Ditto et



605 al., 2023; Mattila et al., 2021; Liu et al., 2024; Klein et al., 2016) may be challenged by the presence of unintended product
 606 ions generated by high concentrations of parent VOCs. For instance, Ernle et al. (2023) recently demonstrated the challenge
 607 of quantifying isoprene from m/Q 69.07 ($C_5H_9^+$) because of interferences from fragments of aldehydes generated from ozone
 608 skin oil oxidation indoors. We briefly demonstrate several challenges related to product ion generation and resulting mass
 609 spectral ambiguity using a measurement of ambient air in a restroom as a case study.

610
 611 High concentrations of terpenoids emitted from fragrant urinal screens reacted with ozone to create oxidized VOCs in the
 612 restroom we sampled from. Fig. 9 shows the selected ion chromatograms for three ions measured, using GC-PTR-ToF-MS,
 613 from the restroom air sample to demonstrate challenges associated with product ion formation.



614
 615 **Figure 9: (a) Selected ion chromatograms (left) of three ions for which PIDs present challenges: $C_3H_9O_2^+$ (top), $C_3H_5O^+$ (middle),**
 616 **and $C_5H_9^+$ (bottom). Dotted vertical lines are placed at the retention times assigned to VOCs or parent ion species either directly**
 617 **measured from calibration sources or supported by time series correlations with known product ions. Peak assignments with an**
 618 **asterisk are species that were assigned from product ion time series analyses. (b) Pie charts showing the ion signal composition with**
 619 **contributions from the VOC typically assigned to the ion (black) and contributions from interfering product ions. Product ion**
 620 **contributions to the ion signal are determined by integrating areas of all the major peaks, calculating the relative contribution of**
 621 **each peak to the total area of all the identified peaks, and classifying them by product ion identity.**
 622

623 In the restroom the ion possibly attributable to propylene glycol, $C_3H_9O_2^+$ (Hopstock et al., 2024), was found to be mostly
 624 comprised of the acetone water cluster. Acetone generates a water cluster with a roughly 10 % efficiency in the Lab 1
 625 instrument used for this restroom measurement. Acetone concentrations are generally elevated indoors, compared to outdoors,



626 and in the restroom acetone concentrations were elevated at approximately 20 nmol mol⁻¹ (equivalent to 20 parts-per-billion).
627 Recent studies have used PTR-MS for the measurement of VOCs, including propylene glycol, in the smoke of electronic
628 cigarettes (Bielik et al., 2024; Hopstock et al., 2024; Sheu et al., 2020). Sheu et al. (2020) could not quantify possible
629 contributions of propylene glycol to thirdhand smoke indoors because of the acetone water cluster interference. This C₃H₉O₂⁺
630 interference from acetone water cluster may be most pronounced indoors where air can contain elevated acetone concentrations
631 from human breath and materials emissions (Molinier et al., 2024).

632

633 Acrolein (C₃H₄O) is a hazardous indoor air pollutant (Seaman et al., 2007; Logue et al., 2011) and recently was measured,
634 using PTR-MS, from a residential test facility (Arata et al., 2021) where concentrations were high enough such that it was the
635 largest source of gas-phase hazardous exposure (Hodshire et al., 2022). In the restroom the C₃H₅O⁺ ion signal (i.e., the H⁺
636 adduct ion commonly attributed to acrolein) experienced considerable interferences from fragmentation of VOCs containing
637 nine (C₉) to twelve (C₁₂) carbon atoms. There were some additional interferences from unidentified sources—one of which
638 may be the propanal hydride transfer product (could not confirm here due to coelution of acetone). In the restroom where
639 terpenoid (monoterpenes, monoterpene alcohols, and monoterpene acetate esters) concentrations were roughly 20 nmol mol⁻¹
640 the fragmentation of two ions likely attributable to terpenoids, C₁₀H₂₁O⁺ and C₁₀H₂₁O₂⁺, make important contributions (56 %)
641 to the C₃H₅O⁺ ion signal. We note that the terpenoids emitted from the urinal screens created high concentrations that may
642 uniquely impact the C₃H₅O⁺ signal compared to other indoor environments. However, this observation points to the possible
643 unexpected impact of consumer product emissions on indoor air measurements of acrolein.

644

645 Isoprene has a history of being difficult to quantify from PTR-MS measurements (e.g., urban air influenced by cooking
646 emissions (Coggon et al., 2024), seawater (Kilgour et al., 2024), and biogenic emissions (Vermeuel et al., 2023)) mostly from
647 fragmentation of aldehydes, but also from the dehydration of 2-methyl-3-buten-2-ol (MBO) measured from coniferous forests.
648 Similar to C₃H₅O⁺ we show that fragments of the terpenoid ions, C₁₀H₂₁O⁺ and C₁₀H₂₁O₂⁺, also make important contributions
649 (80 %) to the C₅H₉⁺ ion signal (Fig. 9). Given the ubiquity of the ions highlighted here indoors, terpenoid presence is another
650 factor that can impact PTR-MS isoprene quantification indoors.

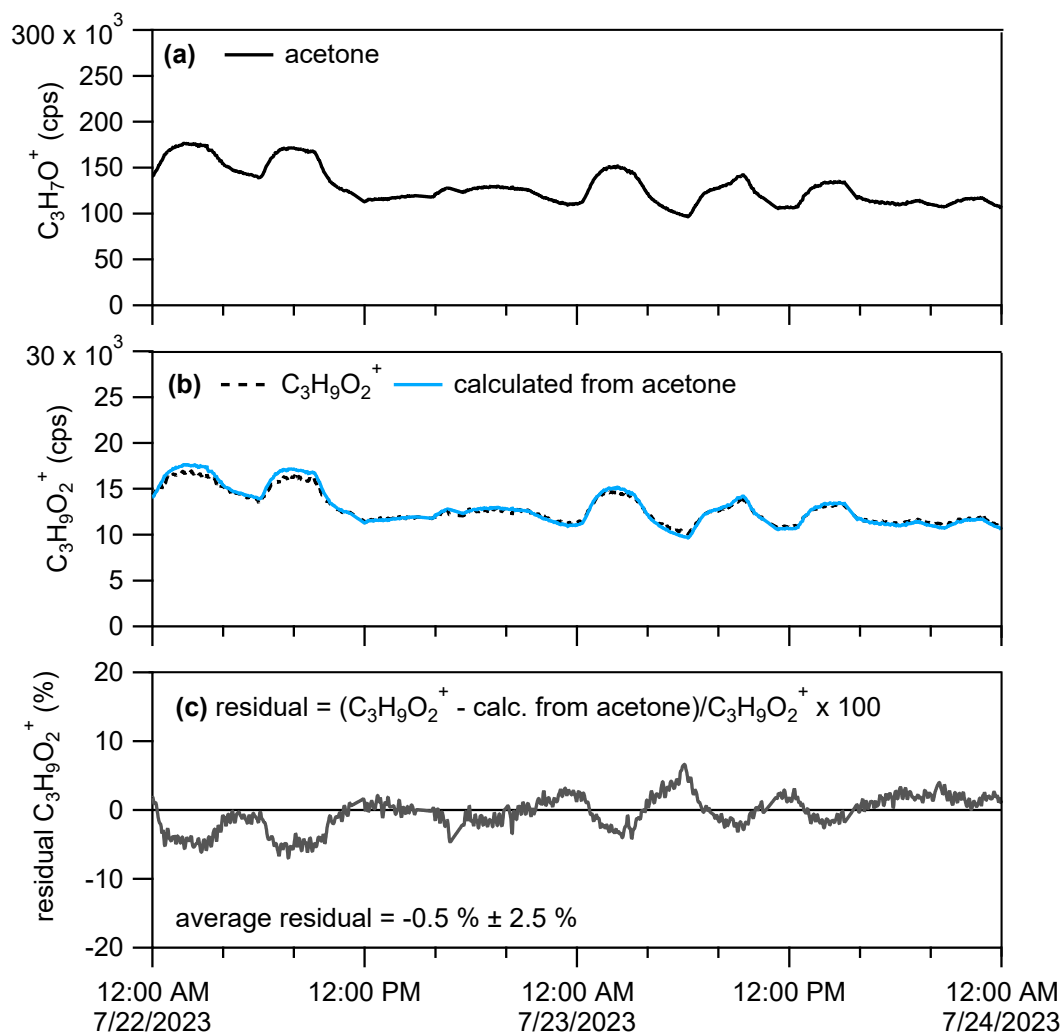
651 3.5 Using PIDs to Improve Identification and Quantification of VOCs from PTR-MS Measurements

652 3.5.1 Method 1: Estimating Product Ion Abundance from Real-Time Data

653 In Section 3.4 we demonstrated the interference of acetone water cluster on the ion signal, C₃H₉O₂⁺, that might be typically
654 attributed to propylene glycol (Fig. 9) using a chromatographic pre-separation. If a PID has been measured from a calibration
655 source, it can be used to estimate the abundance of product ions to an ion signal relative to another ion from real-time data.
656 For example, we can determine the influence of acetone water cluster on the C₃H₉O₂⁺ ion signal measured by the PTR-MS,
657 without chromatographic pre-separation (“real-time data”), by calculating the expected contribution predicted by the acetone



658 PID. We show an example of how we estimated the influence of acetone water cluster on the real-time $C_3H_9O_2^+$ ion signal in
 659 Figure 10.



660
 661 **Figure 10: (a) Time series for $C_3H_7O^+$ attributable to acetone. (b) Time series for $C_3H_9O_2^+$ with the raw signal (black**
 662 **dotted line) and $C_3H_9O_2^+$ calculated to be attributable to acetone water cluster (10 % contribution to acetone PID). (c)**
 663 **Percent residual $C_3H_9O_2^+$ ion signal after subtracting out the estimated contribution from acetone water cluster.**

664
 665 We measured the PID for acetone (as shown in Fig. 8 and listed in the H_3O^+ PID library) as 0.90 H^+ adduct ($C_3H_7O^+$) and 0.10
 666 water cluster ($C_3H_9O_2^+$). Assuming contributions of isomers or product ions to the $C_3H_7O^+$ signal are negligible, we can divide
 667 the product ion fraction for $C_3H_9O_2^+$ ($f_{[MH \cdot H_2O]^+}$) by the product ion fraction for $C_3H_7O^+$ (f_{MH^+}) to get the fraction of acetone



668 water cluster relative to acetone H⁺ adduct ($\frac{f_{[MH\cdot H_2O]^+}}{f_{MH^+}}$). We can then multiply this fraction by the C₃H₇O⁺ signal (S_{MH^+}) to get
 669 the contribution of acetone water cluster to the C₃H₉O₂⁺ signal ($S_{[MH\cdot H_2O]^+}$) following Equation 2,

$$670 \quad S_{[MH\cdot H_2O]^+} = S_{MH^+} \cdot \frac{f_{[MH\cdot H_2O]^+}}{f_{MH^+}} \quad (2)$$

671 Multiplying the C₃H₇O⁺ signal (shown in Fig. 10a) by $\frac{f_{[MH\cdot H_2O]^+}}{f_{MH^+}}$ (i.e., 0.10/0.90 \approx 0.11) generates an estimated C₃H₉O₂⁺ ion
 672 signal time series (Fig. 10b, blue trace) that is from the acetone water cluster. In Fig. 10c we calculate the percent residual
 673 C₃H₉O₂⁺ signal, after subtracting out the estimated contribution of acetone water cluster. The average residual of -0.5 %
 674 indicates that nearly all of the C₃H₉O₂⁺ ion signal measured from the restroom is from acetone water cluster which is consistent
 675 with what we measured from the chromatographic separation in Fig. 9a. Although not shown in this example of C₃H₉O₂⁺, if
 676 after applying this method residual signal remained, and was consistently above zero, that could indicate ion signal related to
 677 H⁺ adducts of VOCs or influences of other product ions. We verified that the C₃H₇O⁺ signal we measured from the restroom
 678 (using GC) was > 95 % (with some possible contribution from propanal and contributions of fragment ions) attributable to
 679 acetone thus suggesting that application of this method may work best when supplemented with a GC measurement.

680
 681 We point to the study of Coggon et al. (2024) for further demonstrations of how to separate the influence of product ions on
 682 H⁺ adduct ions for benzene (C₆H₇⁺), isoprene (C₅H₉⁺), and ethanal (acetaldehyde, C₂H₅O⁺) measured from outdoor air
 683 influenced by oil and gas and cooking emissions. When directly measuring PIDs using a calibration source is not possible, the
 684 H₃O⁺ PID library included with this manuscript can serve as a useful source for estimating possible product ion interferences.
 685 The existing PTR library compiled by Pagonis et al. (2019) contains measurements of fragment product ions that can also
 686 provide product ion data relevant for instruments other than the Vocus. This product ion estimation method may produce
 687 reasonable results for some VOCs like acetone, but many ions will often have multiple isomers or isobaric product ion
 688 interferences that challenge accurate application of the method.

689 3.5.2 Method 2: Using Product Ions for Quantification

690 PTR-MS quantification is often performed using calibrations of an H⁺ adduct signal for a target VOC (e.g., C₃H₇O⁺ for
 691 acetone), but the PTR-MS can also be calibrated to product ions. Coggon et al. (2024) showed that benzene concentrations
 692 calculated from the charge transfer product ion (C₆H₆⁺) calibration agreed with concentrations quantified from GC
 693 measurements. The authors concluded that the benzene charge transfer product ion (C₆H₆⁺), which had no interferences, was
 694 a more suitable signal to quantify benzene from than the H⁺ adduct (C₆H₇⁺), which suffered interferences from fragmented
 695 aromatics. However, pre-separation was used in that study to verify the charge transfer product was free of interferences. In
 696 principle, any product ion that is free of interferences could be used as an alternative to the H⁺ adduct for quantification.



697 3.5.3 Method 3: Supplemental Measurement with a GC

698 It is worth acknowledging the value of a supplemental measurement using GC. When directly interfaced to the PTR-MS, GC
699 can be used to measure PIDs and aid in identifying ion signals from the real-time PTR-MS measurement. Benchtop GCs
700 optimized for thermal desorption measurements can also be used in offline analysis to identify possible sources of ion
701 interferences. Although not discussed here, isomers are confounding influences on the interpretation of ion identities and GC
702 is also useful for quantification of VOC isomers. Nevertheless, not all VOCs present in an air sample are likely to be
703 independently separated (e.g., sesquiterpenes for mid-polarity columns) or trapped and desorbed via a preconcentration system.

704 3.6 Recommendations for Mitigating Challenges from Unintended Product Ion Generation

705 As demonstrated in the interlaboratory comparison data, PTR-MS users are likely to experience unintended product ion
706 generation under a variety of instrument operating conditions. We recommend several practices that PTR-MS users can adopt
707 to improve the interpretability of PTR-MS data:

- 708 ▪ Measure PIDs regularly: Surrogate analytes can be used (and included in calibration source cylinders) to provide
709 some indication of how likely it is a mass spectrum may be influenced by certain types of product ions. For example,
710 benzene can be used as a surrogate for charge transfer reaction chemistry, acrolein (data shown in the H₃O⁺ PTR PID
711 Library) for water clustering, and α -pinene for fragmentation. Because PIDs can change over time, regularly (at least
712 once a month during periods of active measurements) measuring the PIDs of a few key surrogates can provide relative
713 information on how the PIDs of other VOCs may also be changing. The ion chemistry presented in Table 1 can act
714 as a guide for users to evaluate if ions appearing in a mass spectrum could be generated from unintended product
715 ions. Additionally, the step-by-step procedure outlined in the Supplement can serve as a method for measuring PIDs.
- 716 ▪ Optimize analyte detection with instrument tuning: Here we demonstrated IMR E/N and BSQ voltage affected PIDs.
717 A user can measure the PID of target analytes and scan E/N and BSQ voltage values to optimize the production of a
718 desired product ion (e.g., the H⁺ adduct). Because cluster and fragmentation product ions are generated and detected
719 more efficiently at different extremes of E/N and BSQ voltage values instrument tuning will not eliminate unintended
720 product ion generation.
- 721 ▪ Refer to the H₃O⁺ PTR PID Library: For the VOCs available in the library a user can identify problematic m/Q and
722 elemental formula associated with unintended product ions from VOCs known to be in a sample (including multi-
723 component calibration sources).
- 724 ▪ Measure the instrument sample flowrate regularly: We provide evidence suggesting an influence of flowrate on PIDs,
725 but we also note that the sample flowrate will also affect instrument sensitivity (Jensen et al., 2023). When sampling
726 from pristine environments measuring the sample flow once a week may be sufficient. For measurements of urban or
727 indoor air measuring the flow once a day is recommended. Higher frequency flow checks may be necessary for



728 measurements where particulate matter loading is high (e.g., fire research laboratory burn samples, cooking
729 emissions, etc.).

- 730 ▪ If possible, use a supplemental measurement, GC or otherwise, to support identification of ions measured with PTR-
731 MS from multi-component air samples.
- 732 ▪ Define the acceptable level of accuracy for your measurement: PTR-MS provides high time resolution measurements
733 of VOCs in air that cannot be achieved with many techniques. For non-targeted analyses, identifying and accounting
734 for all influences of unintended product ions is currently impractical. Studies that seek to quantify all VOCs measured,
735 both known and unknown, by the PTR-MS may suffer from greater uncertainties arising from unintended product ion
736 generation. While more uncertain, these non-targeted analyses are important for progressing research. On the other
737 hand, users seeking to quantify specific VOCs (e.g., air toxics or hazardous air pollutants) for the purposes of
738 compliance measurements will need to account for product ion chemistry for high accuracy measurements.

739 4 Summary and Conclusions

740 Here we outlined general rules for identifying possible product ion interferences based on common reaction mechanisms that
741 can occur when using PTR-MS. Additionally, the method of product ion classification (using ion formula predicted from
742 mechanisms) used here can be employed in future studies to continue to develop product ion libraries using a consistent
743 methodology so that PIDs can be compared directly from different studies. Consistent with the decades of previous research,
744 which includes measurements on PTR-MS instruments that use a drift tube for ionization, we observe E/N as a predictor of
745 the extent clustering or fragmentation product ions contribute to the PID of a VOC. Of particular importance for the instruments
746 in this study, is also the influence of the BSQ RF voltage affecting PIDs through mass-discrimination.

747
748 We demonstrate here that instrument tuning can affect PIDs, but tuning can also affect instrument sensitivity. We do not
749 discuss the relationship between instrument tuning, product ion formation, and instrument sensitivity here, but instead point
750 the reader to Li et al. (2024) for a detailed evaluation of this relationship relevant for Vocus PTR-ToF-MS instruments.
751 However, we note that specific instrument tuning properties explored here have implications for instrument sensitivity. For
752 instance, Li et al. (2024) showed that the H⁺ adduct contribution to the PID and sensitivity for 1,3,5-trimethylbenzene did not
753 change appreciably with increasing E/N whereas the H⁺ adduct contribution to the PID and sensitivity for hexanal (PID shown
754 here in Fig. 8) decreased with increasing E/N. This comparison demonstrates that VOCs susceptible to fragment ion formation
755 may show decreasing sensitivity to the H⁺ adduct with increasing E/N. In another example, we demonstrated that higher BSQ
756 voltages can filter out lower m/Q ions and affect measured PIDs, but another implication of higher BSQ voltages is that the
757 sensitivity of the H⁺ adduct for lower molecular weight species (e.g., formaldehyde, acetonitrile, formic acid, etc.) will also
758 decrease. Interlaboratory comparisons focusing on constraining the relationship between PIDs and instrument sensitivity



759 would be informative for the development of standard tuning configurations optimized for the measurement of specific VOCs
760 or types of VOCs (e.g., aldehydes, aromatics, etc.).

761
762 Despite having similar operating conditions (i.e. similar E/N and BSQ voltage settings), PIDs measured across laboratories
763 showed considerable variability. Further, PIDs measured from the same instrument over time were not consistent. Our
764 observations support the conclusion that if a user configures the same model PTR-MS identically to an instrument in the
765 literature, they should not expect identical PIDs. Additionally, a user may expect different PIDs from the same instrument after
766 several months.

767
768 However, we also show that some of the variability in PIDs between instruments was explainable from qualitative arguments.
769 For example, Lab 6 operated with the highest E/N and showed the largest contributions of fragmentation and charge/hydride
770 transfer products to PIDs and small contributions from water clusters compared to the other labs. Qualitative arguments based
771 on E/N or BSQ voltage could not completely explain the variation in water clustering between labs. The quantitative constraints
772 on PIDs presented here could be improved with continued input of data from users to the H₃O⁺ PID library (included here as
773 a supplemental document). Future work from our group at NIST will focus on integrating measurements of PIDs contained in
774 the existing PTR library from Pagonis et al. (2019) with the H₃O⁺ PID library included here. We encourage users to continue
775 to contribute data for inclusion in the H₃O⁺ PID library in continued efforts to understand PIDs and standardize methods of
776 PTR-MS measurements.

777 **5 Outlook**

778 All reagent ions used for chemical ionization mass spectrometry create unintended product ions that can present challenges
779 when identifying and quantifying VOCs. Continued work characterizing and constraining the impact of instrument operating
780 parameters and sampling methods on product ion generation is warranted to leverage the sensitivity, selectivity, and versatile
781 sampling capabilities that field-deployable chemical ionization mass spectrometers provide. PTR-MS users should be aware
782 that product ion generation (of not only fragments but also charge/hydride transfer and water clusters) occurs for most VOCs
783 to varying degrees. Additionally, the ambiguity created from product ion contributions to mass spectra measured from
784 chemically complex samples may create challenges to accurate identification and quantification of VOCs—particularly for
785 non-targeted analyses. Further characterization of PIDs across many PTR-MS instruments may be useful in constraining
786 interferences and decreasing the uncertainty from their influence on mass spectra.

787
788 There is a current interest to develop standardized methods of measurement using chemical ionization mass spectrometers.
789 Currently, no standard methods for sampling with PTR-MS or other chemical ionization instruments exists. Notable research
790 efforts towards standardization methods of PTR-MS measurements include the development of ion libraries (Pagonis et al.,



791 2019; Yáñez-Serrano et al., 2021), calibrations and standard reference materials (Worton et al., 2023; Jensen et al., 2023;
792 Sekimoto et al., 2017), data analysis methods (Holzinger, 2015; Cubison and Jimenez, 2015), and interlaboratory comparison
793 studies (Holzinger et al., 2019). Continued efforts, particularly in the form of coordinated interlaboratory comparison studies,
794 would be useful for the development of standard operational procedures and practices.

795 **Supplement**

796 Additional analyses of instrument configuration on PIDs are presented in the supplement. A spreadsheet containing the PID
797 data from the interlaboratory comparison (the “H₃O⁺ PID Library”) is included as a supplemental document. Users wishing to
798 submit data to this library can email the corresponding author (michael.f.link@nist.gov) and a link to submit a data file will
799 be provided in a follow-up email. More details can be found in the “ReadMe” tab of the supplemental H₃O⁺ PID Library.

800 **Competing Interests**

801 The contact author has declared that none of the authors has any competing interests.

802 **Acknowledgements**

803 We would like to acknowledge the National Research Council Research Associateship Program and Alfred P. Sloan
804 Foundation (G-2019-11404) for funding. This material is partially supported by the U.S. Department of Energy (DOE), Office
805 of Science, Office of Biological and Environmental Research, Atmospheric System Research (ASR) under Award No. DE-
806 SC0021985.

807 **Disclaimer**

808 Certain equipment, instruments, software, or materials, commercial or non-commercial, are identified in this paper in to specify
809 the experimental procedure adequately. Such identification is not intended to imply recommendation or endorsement of any
810 product or service by NIST, nor is it intended to imply that the materials or equipment identified are necessarily the best
811 available for the purpose.

812 **References**

813 Antony Joseph, M. J., McIntosh, D. G., Gibson, J. R., and Taylor, S.: Effects of the source gap on transmission efficiency of
814 a quadrupole mass spectrometer, *Rapid Communications in Mass Spectrometry*, 32, 677-685, 2018.
815 Arata, C., Misztal, P. K., Tian, Y., Lunderberg, D. M., Kristensen, K., Novoselac, A., Vance, M. E., Farmer, D. K., Nazaroff,
816 W. W., and Goldstein, A. H.: Volatile organic compound emissions during HOMEChem, *Indoor Air*, 31, 2099-2117, 2021.



- 817 Bielik, N., Correia, D., Rodrigues Crespo, K., Goujon-Ginglinger, C., and Mitova, M. I.: Pitfalls in the Detection of Volatiles
818 Associated with Heated Tobacco and e-Vapor Products When Using PTR-TOF-MS, *Journal of the American Society for Mass*
819 *Spectrometry*, 35, 1261-1271, 10.1021/jasms.4c00062, 2024.
- 820 Breitenlechner, M., Fischer, L., Hainer, M., Heinritzi, M., Curtius, J., and Hansel, A.: PTR3: An Instrument for Studying the
821 Lifecycle of Reactive Organic Carbon in the Atmosphere, *Analytical Chemistry*, 89, 5824-5831,
822 10.1021/acs.analchem.6b05110, 2017.
- 823 Brophy, P. and Farmer, D. K.: Clustering, methodology, and mechanistic insights into acetate chemical ionization using high-
824 resolution time-of-flight mass spectrometry, *Atmospheric Measurement Techniques*, 9, 3969-3986, 2016.
- 825 Buhr, K., van Ruth, S., and Delahunty, C.: Analysis of volatile flavour compounds by Proton Transfer Reaction-Mass
826 Spectrometry: fragmentation patterns and discrimination between isobaric and isomeric compounds, *International Journal of*
827 *Mass Spectrometry*, 221, 1-7, 2002.
- 828 Claflin, M. S., Pagonis, D., Finewax, Z., Handschy, A. V., Day, D. A., Brown, W. L., Jayne, J. T., Worsnop, D. R., Jimenez,
829 J. L., and Ziemann, P. J.: An in situ gas chromatograph with automatic detector switching between PTR-and EI-TOF-MS:
830 isomer-resolved measurements of indoor air, *Atmospheric Measurement Techniques*, 14, 133-152, 2021.
- 831 Coggon, M. M., Stockwell, C. E., Claflin, M. S., Pfannerstill, E. Y., Xu, L., Gilman, J. B., Marcantonio, J., Cao, C., Bates, K.,
832 and Gkatzelis, G. I.: Identifying and correcting interferences to PTR-ToF-MS measurements of isoprene and other urban
833 volatile organic compounds, *Atmospheric Measurement Techniques*, 17, 801-825, 2024.
- 834 Cubison, M. J. and Jimenez, J. L.: Statistical precision of the intensities retrieved from constrained fitting of overlapping peaks
835 in high-resolution mass spectra, *Atmospheric Measurement Techniques*, 8, 2333-2345, 10.5194/amt-8-2333-2015, 2015.
- 836 De Gouw, J. and Warneke, C.: Measurements of volatile organic compounds in the earth's atmosphere using proton-transfer-
837 reaction mass spectrometry, *Mass spectrometry reviews*, 26, 223-257, 2007.
- 838 De Gouw, J., Warneke, C., Karl, T., Eerdekens, G., Van der Veen, C., and Fall, R.: Sensitivity and specificity of atmospheric
839 trace gas detection by proton-transfer-reaction mass spectrometry, *International Journal of Mass Spectrometry*, 223, 365-382,
840 2003.
- 841 Ditto, J. C., Crilley, L. R., Lao, M., Vandenboer, T. C., Abbatt, J. P. D., and Chan, A. W. H.: Indoor and outdoor air quality
842 impacts of cooking and cleaning emissions from a commercial kitchen, *Environmental Science: Processes & Impacts*, 25,
843 964-979, 10.1039/d2em00484d, 2023.
- 844 Ernle, L., Wang, N., Bekö, G., Morrison, G., Wargocki, P., Weschler, C. J., and Williams, J.: Assessment of aldehyde
845 contributions to PTR-MS m/z 69.07 in indoor air measurements, *Environmental Science: Atmospheres*, 3, 1286-1295, 2023.
- 846 Gkatzelis, G. I., Coggon, M. M., Stockwell, C. E., Hornbrook, R. S., Allen, H., Apel, E. C., Bela, M. M., Blake, D. R.,
847 Bourgeois, I., and Brown, S. S.: Parameterizations of US wildfire and prescribed fire emission ratios and emission factors
848 based on FIREX-AQ aircraft measurements, *Atmospheric Chemistry and Physics*, 24, 929-956, 2024.
- 849 Hegen, O., Salazar Gómez, J. I., Schlögl, R., and Ruland, H.: The potential of NO⁺ and O₂⁺ in switchable reagent ion proton
850 transfer reaction time-of-flight mass spectrometry, *Mass Spectrometry Reviews*, 42, 1688-1726, 10.1002/mas.21770, 2023.
- 851 Heinritzi, M., Simon, M., Steiner, G., Wagner, A. C., Kürten, A., Hansel, A., and Curtius, J.: Characterization of the mass-
852 dependent transmission efficiency of a CIMS, *Atmospheric measurement techniques*, 9, 1449-1460, 2016.
- 853 Hodshire, A. L., Carter, E., Mattila, J. M., Ilacqua, V., Zambrana, J., Abbatt, J. P., Abeleira, A., Arata, C., DeCarlo, P. F., and
854 Goldstein, A. H.: Detailed Investigation of the Contribution of Gas-Phase Air Contaminants to Exposure Risk during Indoor
855 Activities, *Environmental science & technology*, 56, 12148-12157, 2022.
- 856 Holzinger, R.: PTRwid: A new widget tool for processing PTR-TOF-MS data, *Atmospheric Measurement Techniques*, 8,
857 3903-3922, 10.5194/amt-8-3903-2015, 2015.
- 858 Holzinger, R., Acton, W. J. F., Bloss, W. J., Breitenlechner, M., Crilley, L. R., Dusanter, S., Gonin, M., Gros, V., Keutsch, F.
859 N., and Kiendler-Scharr, A.: Validity and limitations of simple reaction kinetics to calculate concentrations of organic
860 compounds from ion counts in PTR-MS, *Atmospheric measurement techniques*, 12, 6193-6208, 2019.
- 861 Hopstock, K. S., Perraud, V., Dalton, A. B., Barletta, B., Meinardi, S., Weltman, R. M., Mirkhanian, M. A., Rakosi, K. J.,
862 Blake, D. R., Edwards, R. D., and Nizkorodov, S. A.: Chemical Analysis of Exhaled Vape Emissions: Unraveling the
863 Complexities of Humectant Fragmentation in a Human Trial Study, *Chemical Research in Toxicology*, 37, 1000-1010,
864 10.1021/acs.chemrestox.4c00088, 2024.



- 865 Jensen, A. R., Koss, A. R., Hales, R. B., and De Gouw, J. A.: Measurements of volatile organic compounds in ambient air by
866 gas-chromatography and real-time Vocus PTR-TOF-MS: calibrations, instrument background corrections, and introducing a
867 PTR Data Toolkit, *Atmospheric Measurement Techniques*, 16, 5261-5285, 10.5194/amt-16-5261-2023, 2023.
- 868 Kilgour, D. B., Novak, G. A., Clafin, M. S., Lerner, B. M., and Bertram, T. H.: Production of oxygenated volatile organic
869 compounds from the ozonolysis of coastal seawater, *Atmospheric Chemistry and Physics*, 24, 3729-3742, 10.5194/acp-24-
870 3729-2024, 2024.
- 871 Klein, F., Platt, S. M., Farren, N. J., Detournay, A., Bruns, E. A., Bozzetti, C., Daellenbach, K. R., Kilic, D., Kumar, N. K.,
872 and Pieber, S. M.: Characterization of gas-phase organics using proton transfer reaction time-of-flight mass spectrometry:
873 cooking emissions, *Environmental science & technology*, 50, 1243-1250, 2016.
- 874 Koss, A. R., Warneke, C., Yuan, B., Coggon, M. M., Veres, P. R., and de Gouw, J. A.: Evaluation of NO⁺ reagent ion chemistry
875 for online measurements of atmospheric volatile organic compounds, *Atmospheric Measurement Techniques*, 9, 2909-2925,
876 2016.
- 877 Krechmer, J., Lopez-Hilfiker, F., Koss, A., Hutterli, M., Stoermer, C., Deming, B., Kimmel, J., Warneke, C., Holzinger, R.,
878 Jayne, J., Worsnop, D., Fuhrer, K., Gonin, M., and De Gouw, J.: Evaluation of a New Reagent-Ion Source and Focusing Ion-
879 Molecule Reactor for Use in Proton-Transfer-Reaction Mass Spectrometry, *Analytical Chemistry*, 90, 12011-12018,
880 10.1021/acs.analchem.8b02641, 2018.
- 881 Li, F., Huang, D. D., Tian, L., Yuan, B., Tan, W., Zhu, L., Ye, P., Worsnop, D., Hoi, K. I., and Mok, K. M.: Response of
882 protonated, adduct, and fragmented ions in Vocus proton-transfer-reaction time-of-flight mass spectrometer (PTR-ToF-MS),
883 *Atmospheric Measurement Techniques*, 17, 2415-2427, 2024.
- 884 Li, H., Almeida, T. G., Luo, Y., Zhao, J., Palm, B. B., Daub, C. D., Huang, W., Mohr, C., Krechmer, J. E., and Kurtén, T.:
885 Fragmentation inside proton-transfer-reaction-based mass spectrometers limits the detection of ROOR and ROOH peroxides,
886 *Atmospheric Measurement Techniques*, 15, 1811-1827, 2022.
- 887 Link, M. F., Robertson, R. L., Shore, A., Hamadani, B. H., Cecelski, C. E., and Poppendieck, D. G.: Ozone generation and
888 chemistry from 222 nm germicidal ultraviolet light in a fragrant restroom, *Environmental Science: Processes & Impacts*, 26,
889 1090-1106, 2024.
- 890 Liu, J., Jiang, J., Ding, X., Patra, S. S., Cross, J. N., Huang, C., Kumar, V., Price, P., Reidy, E. K., Tasoglou, A., Huber, H.,
891 Stevens, P. S., Boor, B. E., and Jung, N.: Real-time evaluation of terpene emissions and exposures during the use of scented
892 wax products in residential buildings with PTR-TOF-MS, *Building and Environment*, 255, 111314,
893 10.1016/j.buildenv.2024.111314, 2024.
- 894 Logue, J. M., McKone, T. E., Sherman, M. H., and Singer, B. C.: Hazard assessment of chemical air contaminants measured
895 in residences, *Indoor Air*, 21, 92-109, 10.1111/j.1600-0668.2010.00683.x, 2011.
- 896 Lopez-Hilfiker, F. D., Iyer, S., Mohr, C., Lee, B. H., D'Ambro, E. L., Kurtén, T., and Thornton, J. A.: Constraining the
897 sensitivity of iodide adduct chemical ionization mass spectrometry to multifunctional organic molecules using the collision
898 limit and thermodynamic stability of iodide ion adducts, *Atmospheric Measurement Techniques*, 9, 1505-1512, 2016.
- 899 Materić, D., Lanza, M., Sulzer, P., Herbig, J., Bruhn, D., Gauci, V., Mason, N., and Turner, C.: Selective reagent ion-time of
900 flight-mass spectrometry study of six common monoterpenes, *International Journal of Mass Spectrometry*, 421, 40-50,
901 10.1016/j.ijms.2017.06.003, 2017.
- 902 Mattila, J. M., Arata, C., Abeleira, A., Zhou, Y., Wang, C., Katz, E. F., Goldstein, A. H., Abbatt, J. P., DeCarlo, P. F., and
903 Vance, M. E.: Contrasting Chemical Complexity and the Reactive Organic Carbon Budget of Indoor and Outdoor Air,
904 *Environmental Science & Technology*, 56, 109-118, 2021.
- 905 McCrumb, J. L. and Warneck, P.: On the mechanism of water cluster-ion formation in nitrogen, *The Journal of Chemical*
906 *Physics*, 67, 5006-5011, 10.1063/1.434722, 1977.
- 907 Misztal, P., Heal, M., Nemitz, E., and Cape, J.: Development of PTR-MS selectivity for structural isomers: Monoterpenes as
908 a case study, *International Journal of Mass Spectrometry*, 310, 10-19, 2012.
- 909 Molinier, B., Arata, C., Katz, E. F., Lunderberg, D. M., Ofofiele, J., Singer, B. C., Nazaroff, W. W., and Goldstein, A. H.:
910 Bedroom Concentrations and Emissions of Volatile Organic Compounds during Sleep, *Environmental Science & Technology*, 58,
911 7958-7967, 10.1021/acs.est.3c10841, 2024.
- 912 Müller, M., Mikoviny, T., and Wisthaler, A.: Detector aging induced mass discrimination and non-linearity effects in PTR-
913 ToF-MS, *International Journal of Mass Spectrometry*, 365-366, 93-97, 10.1016/j.ijms.2013.12.008, 2014.



- 914 Pagonis, D., Sekimoto, K., and de Gouw, J.: A library of proton-transfer reactions of H_3O^+ ions used for trace gas detection,
915 *Journal of the American Society for Mass Spectrometry*, 30, 1330-1335, 2019.
- 916 Reinecke, T., Leiminger, M., Jordan, A., Wisthaler, A., and Müller, M.: Ultrahigh Sensitivity PTR-MS Instrument with a Well-
917 Defined Ion Chemistry, *Analytical Chemistry*, 95, 11879-11884, 10.1021/acs.analchem.3c02669, 2023.
- 918 Seaman, V. Y., Bennett, D. H., and Cahill, T. M.: Origin, Occurrence, and Source Emission Rate of Acrolein in Residential
919 Indoor Air, *Environmental Science & Technology*, 41, 6940-6946, 10.1021/es0707299, 2007.
- 920 Sekimoto, K. and Koss, A. R.: Modern mass spectrometry in atmospheric sciences: Measurement of volatile organic
921 compounds in the troposphere using proton-transfer-reaction mass spectrometry, *Journal of Mass Spectrometry*, 56, e4619,
922 2021.
- 923 Sekimoto, K., Li, S.-M., Yuan, B., Koss, A., Coggon, M., Warneke, C., and de Gouw, J.: Calculation of the sensitivity of
924 proton-transfer-reaction mass spectrometry (PTR-MS) for organic trace gases using molecular properties, *International Journal*
925 *of Mass Spectrometry*, 421, 71-94, 2017.
- 926 Sheu, R., Stönnner, C., Ditto, J. C., Klüpfel, T., Williams, J., and Gentner, D. R.: Human transport of thirdhand tobacco smoke:
927 A prominent source of hazardous air pollutants into indoor nonsmoking environments, *Science Advances*, 6, eaay4109,
928 10.1126/sciadv.aay4109, 2020.
- 929 Smith, D., McEwan, M. J., and Španěl, P.: Understanding Gas Phase Ion Chemistry Is the Key to Reliable Selected Ion Flow
930 Tube-Mass Spectrometry Analyses, *Analytical Chemistry*, 92, 12750-12762, 10.1021/acs.analchem.0c03050, 2020.
- 931 Španěl, P. and Smith, D.: SIFT studies of the reactions of H_3O^+ , NO^+ and O_2^+ with a series of alcohols, *International Journal*
932 *of Mass Spectrometry and Ion Processes*, 167-168, 375-388, 10.1016/s0168-1176(97)00085-2, 1997.
- 933 Španěl, P., Doren, J. M. V., and Smith, D.: A selected ion flow tube study of the reactions of H_3O^+ , NO^+ , and O_2^+ with saturated
934 and unsaturated aldehydes and subsequent hydration of the product ions, *International Journal of Mass Spectrometry*, 213,
935 163-176, 10.1016/s1387-3806(01)00531-0, 2002.
- 936 Vermeuel, M. P., Novak, G. A., Kilgour, D. B., Claflin, M. S., Lerner, B. M., Trowbridge, A. M., Thom, J., Cleary, P. A.,
937 Desai, A. R., and Bertram, T. H.: Observations of biogenic volatile organic compounds over a mixed temperate forest during
938 the summer to autumn transition, *Atmospheric Chemistry and Physics*, 23, 4123-4148, 2023.
- 939 Wang, N., Müller, T., Ernle, L., Bekö, G., Wargocki, P., and Williams, J.: How Does Personal Hygiene Influence Indoor Air
940 Quality?, *Environmental Science & Technology*, 2024.
- 941 Warneke, C., De Gouw, J. A., Kuster, W. C., Goldan, P. D., and Fall, R.: Validation of atmospheric VOC measurements by
942 proton-transfer-reaction mass spectrometry using a gas-chromatographic pre-separation method, *Environmental science &*
943 *technology*, 37, 2494-2501, 2003.
- 944 Worton, D. R., Moreno, S., O'Daly, K., and Holzinger, R.: Development of an International System of Units (SI)-traceable
945 transmission curve reference material to improve the quantitation and comparability of proton-transfer-reaction mass-
946 spectrometry measurements, *Atmospheric Measurement Techniques*, 16, 1061-1072, 10.5194/amt-16-1061-2023, 2023.
- 947 Xu, L., Coggon, M. M., Stockwell, C. E., Gilman, J. B., Robinson, M. A., Breitenlechner, M., Lamplugh, A., Crouse, J. D.,
948 Wennberg, P. O., Neuman, J. A., Novak, G. A., Veres, P. R., Brown, S. S., and Warneke, C.: Chemical ionization mass
949 spectrometry utilizing ammonium ions (NH_4^+ CIMS) for measurements of organic compounds in the atmosphere, *Atmospheric*
950 *Measurement Techniques*, 15, 7353-7373, 10.5194/amt-15-7353-2022, 2022.
- 951 Yáñez-Serrano, A. M., Filella, I., Llusà, J., Gargallo-Garriga, A., Granda, V., Bourtsoukidis, E., Williams, J., Seco, R.,
952 Cappellin, L., Werner, C., De Gouw, J., and Peñuelas, J.: GLOVOCS - Master compound assignment guide for proton transfer
953 reaction mass spectrometry users, *Atmospheric Environment*, 244, 117929, 10.1016/j.atmosenv.2020.117929, 2021.
- 954 Yuan, B., Koss, A. R., Warneke, C., Coggon, M., Sekimoto, K., and de Gouw, J. A.: Proton-transfer-reaction mass
955 spectrometry: applications in atmospheric sciences, *Chemical reviews*, 117, 13187-13229, 2017.